APPLICATIONS OF SURFACE DISCHARGE MODELING, SIMULATION AND TESTING TO ELECTRICAL INSULATION SYSTEMS

by

Skyler Schwartz

A Thesis Submitted in
Partial Fulfillment of the
Requirements for the Degree of

Master of Science
in Engineering

at

The University of Wisconsin Milwaukee

May 2023

ABSTRACT

APPLICATIONS OF SURFACE DISCHARGE MODELING, SIMULATION AND TESTING TO ELECTRICAL INSULATION SYSTEMS
by
Skyler Schwartz
University of Wisconsin - Milwaukee, 2023
Under the Supervision of Professor Robert Cuzner

Advances in power electronics and the increasing demand for highly power dense power distribution systems have increased the demands for electrical insulation systems. A critical challenge in insulation system design is the prevention and mitigation of partial discharge which drives premature aging and failure of electrical assets. This work applies and validates a recently proposed model for surface discharge applied to the case of a laminated bus bar. The results from the modeling and testing shows the traditional concept of creepage, while essential for preventing a flashover events provides little insight into surface discharge. The approach to characterize the laminated bus bar provides insight into producing partial discharge free designs as a result of modeling. However, in many applications various stresses and conditions could result in partial discharge inception during the assets life, even if partial discharge is not present at commissioning. This motivates the selection of a candidate material which can endure partial discharge to some extent. In this pursuit an approach for rapid material characterization is explored through the testing of commercially available Corona Resistant Kapton (Kapton CR) and Non-Corona Resistant Kapton (Kapton NCR).

DEDICATION

First, I would like to thank my Advisor and Professor Robert Cuzner for the opportunities to learn and grow as an engineer. I would also like to thank my family for their unconditional support, without it I would have never made it to this point in my educational journey. I would also like to thank all of my Colleagues in the lab for making the process of graduate school a truly enjoyable experience. In particular I would like to thank Debashish Nath for support in the many long days of research which made this work possible. I also would like to thank all of my colleagues at ATC, especially Cris Kramschuster and Carl Schutz for motivating me to continue to learn in the area of power systems.

TABLE OF CONTENTS

LIST OF FIGURES

LIST OF TABLES

ACKNOWLEDGEMENTS

This research was conducted under Office of Naval Research, grant N00014-21-1-2124, Office of Naval Research, Grant No. N00014-18-1-2622 and was approved for public release. This work was also made possible due to the support from Professor Montanari and the opportunity to study, learn and conduct research in the areas of partial discharge and insulation systems.

Chapter 1

Introduction

Wide band-gap based power electronics have resulted in greater electric field stresses on electrical insulating systems due to the higher switching frequency and increased demand for highly power-dense modules. These greater stresses can increase the risk of partial discharges which drives premature aging of insulation systems[35, 43]. The critical factor which determines the rate of aging is the source and type of partial discharge (internal, surface or corona) present. To mitigate the risk for insulation failure insulation designs typically rely on standards which define insulation categories, creepage, clearance and testing requirements. Creepage and clearance refer to the required minimum distances along the surface of an insulator and distance through air between electrical terminals (terminal spacing). Creepage and clearance requirements are accounted for during insulation system design and are necessary to prevent a destructive flashover event but provide little insight into the probability of partial discharge inception [36]. To account for this limitation standards require several different types of tests for insulation systems to mitigate the risk of failure under various operating conditions. Standards typically require specific testing to ensure that partial discharges will not normally occur, this however is not an optimal solution as testing does not produce results until after a prototype has been designed and built. Limitations of testing has motivated investigation into the underlying physics and modeling for partial discharge[37, 36]. Specifically, previous work has proposed a theoretical foundation for modeling of internal partial discharge and much more recently for surface discharges. The models of both types of partial discharge may provide greater insight into predicting sources of partial discharge at the design stage.

One technology used as a result of power electronics is a laminated bus bar where bus layers are brought close together and embedded in insulation. Laminated bus bars are used to minimize parasitic bus inductance of which power electronic converters are particularly susceptible. Specifically, parasitic inductance drives

losses for power electronic based converters, and has also been shown to impact Electromagnetic Interference (EMI) produced by the converters. Laminated bus bars have a particular risk for aging and failure due to partial discharge, which motivates this work to characterize the performance of a laminated bus bar. One key part of this characterization is to provide an understanding of surface discharge through the application of theory, simulation and testing. The ultimate goal of the analysis is to understand which factors influence surface discharge inception[2, 28].

An important design objective of an insulation system is to ensure partial discharge will not occur during normal operation. However, it may not always be possible to ensure a partial discharge free design when environmental conditions vary. Most power system applications are located in environments which are not perfectly controlled, and it is possible that pollution, mechanical or thermal stresses over time could result in a change which would allow for partial discharge inception. To mitigate this risk a proper insulating material should be selected during insulation design, which has motivated much work in material development. The choice of an insulator will depend on many factors one of which should be partial discharge endurance especially in applications with uncontrolled environments. In this pursuit an approach which allows for rapid material characterization using surface erosion testing will be investigated as a tool to allow for better design decisions between candidate materials without months or years of testing[34].

1.1 Power Systems Background

Power distribution systems are designed to transfer power from the location of generation to loads at the demand of an end user. Power systems generally are comprised of a high voltage transmission system, a medium voltage distribution system and a low voltage network. High or medium voltage systems are employed to reduce electrical losses as a result of transmitting electricity through imperfect conductors across long (or medium) distances. The key trade-off of operating power systems at high or medium voltages is the higher electric fields which results in greater insulation requirements and larger air gap distances in order to prevent flash over events. These occur due to insufficient insulation or as a result of insulation failure. A power system is comprised of many sub components which include (but are not limited to): transmission lines, distribution lines, transformers, circuit breakers, auxiliary transformers and protective relays. Traditionally the grid has been comprised of synchronous generation at 50 Hz or 60 Hz with minimal saturation of solid state devices. Recently the application of solid state power electronic devices have increased due to penetration of solar, wind, battery storage, and variable speed drive systems. Each of which often include a medium voltage DC link.

Several important objectives of the power systems are efficient power delivery, reliability, and human

safety. To minimize cost, power should be delivered with minimal losses (maximum possible efficiency), and with minimal power disruptions (faults, outages or failures) all while minimizing safety risks. Both minimizing power disruption and ensuring a safe operation of the power system relies on insulation system design. Insulation failure can result in a fault which causes a service discontinuity, or even the complete failure of electrical equipment such as a transformer, generator or motor. Insulation failure can also result in an arc flash event which is the greatest risk for an electrically related injury. To prevent these worst case scenarios standards are typically employed in the design and testing of equipment and more generally power systems.

1.2 Approach and Motivation - A Virtual Prototyping Process

The background and motivation for this work is based on a virtual prototyping process for power electronic equipment. The virtual prototyping process is an approach to build up optimal drawers, cabinets, and bays of power electronics which account for dimensions of insulation, thermal management and accessibility. The approach was proposed by Cuzner et. al. [11] for shipboard design space exploration as it allows for system level design and a tool for evaluating state of the art technology. During the shipboard system design process many decisions are made, and it is essential that decisions are made based on optimal solution to ensure the best possible design and best possible technologies. What makes this process more complicated is the fact that objectives of optimization often compete. For example a more efficient system may be more expensive then a slightly less efficient system=. To address this issue and to ensure an optimized shipboard design the virtual prototyping process is employed based on metamodels for different parts of the shipboard system. These metamaodels contain the information relating to the physical characteristics of the equipment (*e.g.* weight, power density etc.) while accounting for all of real world considerations in building up the drawers, cabinets, and bays [10]. Optimization if completed at the component level cannot guarantee an optimal system level design. Optimization at the system level is preferable to component level optimization as it can include allocations that only exist at the system level including insulation require1ments and thermal requirements. As the voltages increase the impact on power density of insulation allocations grows significantly, this trade off is only seen at the system level. To current approach to scaling is based on standards which will assign the type of solid insulation required as well as creepage and clearance distances. These standards have a level of conservatism, and as an allocation are a placeholder for physics based models. In order to produce an optimal design there must be a mathematical description of the physics. This work intends to lay the foundation for these physics based models which can then be Incorporated into the virtual prototyping process.

In the design of the power systems each of the modules used should be optimized to the requirements set by stakeholders. Typically hover optimization is completed at the component level, leaving ambiguity about the impact of the design at the system level. The virtual prototyping process allows for optimization to be done at the system level ensuring that any selected design will meet the stakeholder requirements.. Two of the largest drivers of the sizing of shipboard electrical components are thermal requirements and insulation coordination which are in fact often competing.

The virtual prototyping process approach is shown in Figure 1.1, where physics based models or allocations are feed into the model. These models are used to build up the dimensions of the cabinets. Inputs from stakeholders will determine the system design space exploration variables along with requirements and constraints.

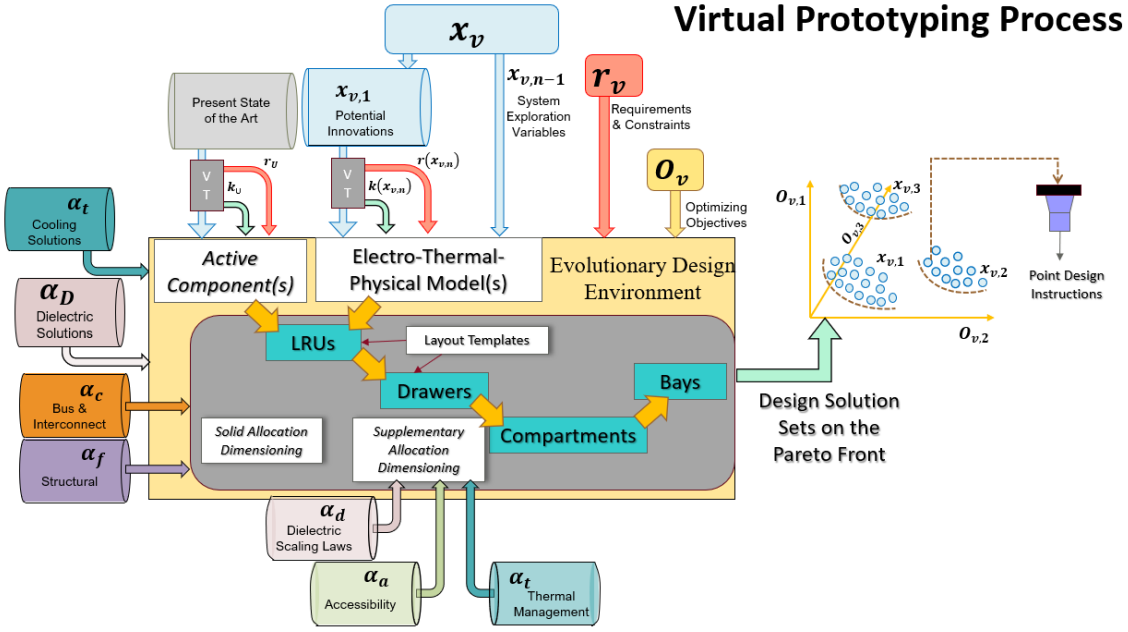

Figure 1.1: Virtual Prototyping Process Overview

1.3 Insulation Coordination

Insulation Coordination is the process of designing an insulation system to meet the requirements of the applications. Typically insulation coordination is completed by application of an industry standard such as IEEE Std C62.82.1™-2010, UL 1446, and/or IEC 61800-5 which provide required insulation levels as a function of voltage and application[19, 47, 1]. Two terms which are frequently referred to in insulation coordination are creepage and clearance. Creepage refers to the distance between terminals of different voltage measured across an insulating surface. Clearance refers to the distance between two terminals of

different voltage measured directly through air shown pictorially by Figure 1.2.

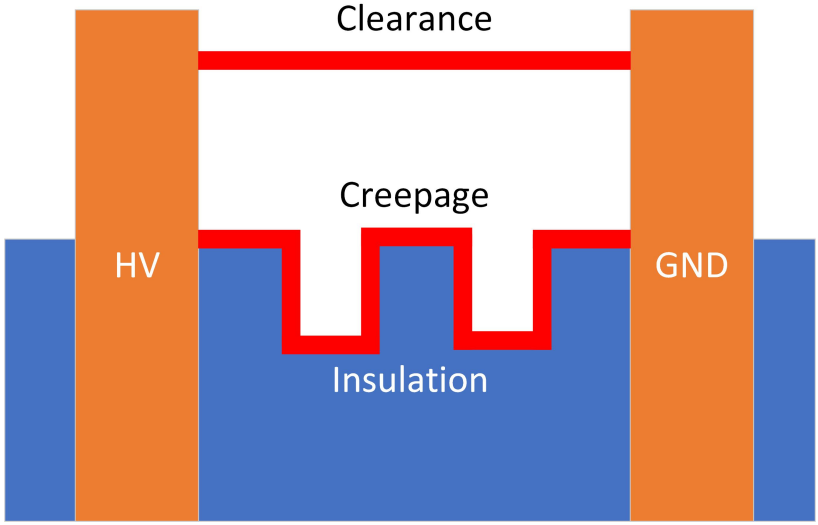

Figure 1.2: Definition of Creepage and Clearance

Often standards require insulation testing which includes lightning insulation testing to ensure survival if the equipment is struck by lighting. Another common test completed for insulation systems is partial discharge testing. Partial discharge is the localized failure of an insulating gas such that a sufficient amount of gas ionizes and forms a partial conducting bridge between electrical terminals. Partial discharge can be particularly harmful for insulation systems and cause premature aging and failure[28]. As a result partial discharge testing is often required, and the specific testing will depend on the application (Transformers, Cables, Switchgear, etc.). The relevant Standard on the partial discharge testing while sharing many commonalities will vary depending on the application.

In particular IEC 61800-5 while specifically intended for medium voltage motor drive systems has been proposed in literature to apply more generally for medium voltage power systems which rely on power electronics [10]. The basic approach for insulation coordination layout out by the standard is as follows for grounded power systems:

The overvoltage category for the device under test will be selected based on the RMS line to ground voltage. After calculation of the overvoltage category the requirements for insulation coordination are driven by the general type of insulation. There are three insulation types; functional insulation which is insulation that is required for the reliable operation of the asset but not sufficient for protection against shock hazards. Second is basic insulation which provides protection against shock hazards. Third is supplemental insulation which provides shock protection even if the basic insulation fails. Fourth and finally is reinforced insulation which is the combination of basic and supplemental insulation. The overvoltage category, the type of

insulation, and the environment of the insulator will all determine the creepage and clearance requirements which are table driven). Once the insulation has been laid out according to the standards several tests are required to ensure the insulation will function properly. The standards layout many of these, but the two most relevant to partial discharge are the impulse voltage test and the partial discharge test. The impulse voltage test is a high frequency pulse applied to the insulation system which is intended to account for atmospheric and switching impulses. This test is a breakdown test, as the insulation passes if it survives the test. The second test is a partial discharge test which applies a voltage according to Figure 1.3. V_PD is the maximum applied voltage across the insulation system under test. In order for the insulation to pass this test any measured partial discharge must be below 10pC of apparent charge. [1]

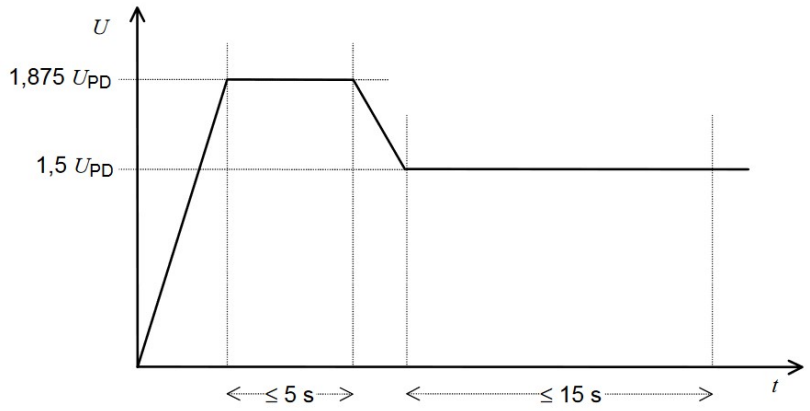

Figure 1.3: Partial Discharge Test per IEC 61800-5 [1]

One assumption of the standard is that any manufacturing defects in the bulk of an insulator are small and are able to be manufactured such that partial discharge will not take place. A similar assumption is made for creepage requirements which are based on minimizing the probability of a surface flashover event taking place between terminals. It is still possible for surface discharges to take place at the electrode,air and insulator triple point which will not cause a flashover event but may result in a partial discharge test failure. Thus predicting partial discharge instead of reacting to it during the testing phase is an essential objective[33]. Solid electrical insulating materials are broadly classified into two categories organic, and inorganic insulators (with and without carbon). Examples of organic insulators would by (cross-linked polyethelene) XLPE, polycarbonate or any other polymeric insulation. Inorganic insulators would be glass, porcelain or other ceramic insulators. Organic insulators typically have applications in cables, motors and laminated bus bars to name a few due to their often superior properties. Inorganic insulators still have many applications including in the areas of outdoor and particularly high voltage applications [3].

1.4 Laminated Bus Bar

Power electronic based voltage source converters have increased in use as a consequence of IGBTs used in motor drives and power converter applications[2]. One challenge in power converter design is the impact of inductance as the amount of inductance limits the rate of change of current, and it consequently increases the switch losses. This challenge has become even more prevalent with the advent of wide band gap semiconductors which can operate at a higher frequency and with larger dV/dt. The most common approach to limit the inductance is through a laminated bus which is comprised of multiple conductors embedded in an epoxy resin. Due to this structure a laminated bus bar also has the capability to increase the overall power density with the trade off of increased insulation stress particularly at medium voltages[2, 33].

1.5 Thesis Overview and Organization

In chapter 2, this thesis will first establish the state of the art of insulation research and lay the foundation which includes background physics for the work to be presented. The primary motivation of this work is to explore approaches for physical modeling which can be Incorporated into a virtual prototyping process. Next in chapter 3 an investigation of surface discharge inception is conducted through modeling, simulation and testing of a laminated bus bar under AC and DC voltages. In chapter 4 the impact of surface discharge on insulation aging and particularly as a method for material performance evaluation was studied on commercially available Kapton and corona resistant Kapton. Final conclusions and potential future work will be discussed in chapter 5.

Chapter 2

State of the Art of Electrical Insulation Design and Partial Discharge

All dielectric materials have a threshold where if the electric field in the material exceeds the threshold the electrical insulation will begin to conduct and fail. This is a worst case failure mode as the primary function of insulation is to prevent electrical conduction between energized conductors or from an energized conductor to ground. Preventing this failure is a primary driver of the electrical insulation design and coordination to ensure the electric fields in the insulating medium do not fail in order to reliably ensure galvanic isolation. In addition local field enhancements or material defects can cause partial discharges which can cause premature aging and if left unaddressed premature failure. These factors motivate an exploration of the underlying physics and mitigation strategies regarding partial discharge.

2.1 Physical Overview

The specific mechanism which drives the breakdown of gases is fundamentally associated with the ionization and recombination of gas atoms and molecules. Charged particles are present throughout the atmosphere and can occur from cosmic radiation or radioactive elements. Ionization occurs when an electron is provided enough energy (from the aforementioned sources) to be separated from the atom to which it was bound. This results in the production of an additional electron, a negative ion and a positive ion which is the remaining nucleus and bound electrons of the atom. At the same time, ions are much less stable than atoms, and tend to attract any nearby free electrons and can recombine into an atom due to their net charge. These two processes of the removal of an electron and re-absorption of an electron are called ionization and recombination

respectively. Each of these play an important role in the physical processes of breakdown in gases [3, 28].

If a charged particle is in the presence of an electric field (and is free to move) it will be accelerated either toward or away from the source of the electric field (depending on the sign of the charge). In general electric fields can be classified into three major categories. First is uniform electric fields which occur when the spatial dependence of the electric field is zero, or very small (e.g. a parallel plate capacitor). Second are weakly non-uniform fields where there is a spatial dependence of the electric field which is non-uniform but not to the point of a large field divergence (e.g. a charged sphere). Third and finally there are highly non-uniform fields which correspond to a significant field divergence (e.g. a charged needle). Because electric fields provide the force which produces charge acceleration the ionization processes relations can be made directly to the electric field. But it is important to note that fundamentally ionization processes are stochastic processes due to the uncertainty in presence of electrons. Even though the underlying physics is stochastic, often deterministic approximations are used to describe the ionization phenomena.

2.2 Gas Discharges in a Uniform Electric Field

Gas discharges in uniform electric fields are driven by the Townsend Mechanism, which has an ignition condition based on the presence of a large enough electric field. If the electric field is large enough an electron which happened to be present in the electric field will be accelerated. When the accelerated electron collides with another atom in air, it will produce a first generation avalanche. The first generation results in a second electron and a positive ion, both of which are then accelerated in opposite directions. The now two electrons will continue to collide with atoms and produce more accelerating electrons in an exponentially growing process.

While ions are always present in air, typical interactions (due to thermal vibrations) do not have enough kinetic energy to cause ionization from inter-molecular collisions. It is important to note that the electrons (negative ions) have a much smaller mass than gas atoms or gas ions, thus they have a much higher mobility. The result of this higher mobility is a greater rate of acceleration when exposed to an electric field. Positive ions move much slower than electrons, but will eventually collide with the electrode surface, the result of this collision plays an important role in a breakdown event. Positive ions can cause an electron to be emitted when they collide with the high voltage conductor. This electron emission is a relatively low probability event.

The Townsend ignition condition states that gas breakdown will take place when an electron avalanche bridges the gap between electrodes and when a sufficient amount of electrons are produced from the high voltage electrode to propagate the process. The production of electrons through impact ionization is given by

the primary ionization coefficient, and the emission of electrons from the conductor surface is parameterized by the secondary ionization coefficient. Emitted electrons will then become a seed electron for further electron avalanches, forming a positive feedback loop which lays the baseline criteria for breakdown. The breakdown process is defined mathematically. Each ionization generation can be defined by a mathematical series of which divergence correspond to a breakdown event and convergence concludes no breakdown [3].

In deriving the breakdown criteria, begin with the relationship between the number of initial electrons first accelerated by the electric field. If a gap between conductors is of length x the total number of electrons will be:

$$N = N_1 e^{(\alpha-\eta)x} \tag{2.1}$$

Where N is the number of electrons after the avalanche process, N_1 is the number of ignition electrons, α is the ionization coefficient, η is the recombination coefficient, and x is the distance from the initial ignition electron and the ground conductor. Assuming the initial electron is near to the high voltage conductor, the distance x can be replaced with distance d. The second equation relates to the amount of seed electrons present after avalanche n. It is typically assumed that the recombination coefficient η is much smaller than the ionization coefficient (which is true in the case for air at sufficiently high electric fields and at room temperatures).

$$N_n = \gamma^{n-1}(e^{\alpha d} - 1)^{n-1} \tag{2.2}$$

Where γ is the surface ionization coefficient which relates to the quantity of electrons emitted by the impact of a positive ion on the surface of the electrode. The criteria for breakdown in a uniform field is constructed as a geometric series of:

$$N_c = \frac{e^{\alpha d}}{1 - \gamma(e^{\alpha d} - 1)} \tag{2.3}$$

The geometric series has 2 possible scenarios:

Convergence:

$$\gamma(e^{\alpha d} - 1) < 1 \tag{2.4}$$

Divergence:

$$\gamma(e^{\alpha d} - 1) \geq 1 \tag{2.5}$$

If the series diverges then a breakdown will occur, but if the series converges there will not be a breakdown. This means if the amount of seed electrons grows through the avalanche process a positive feedback loop is formed resulting in instability [3].

2.2.1 Electron Generation

The specific geometry and materials present will have an impact on the generation of an initial seed electron which starts the ionization process. The generation of the electrons can come from a materials surface. This process holds true in gases either under atmospheric conditions or enclosed in a cavity[8, 37]. The general classification of electron generation can be broken down into two categories, volume generation and surface generation. The volume generation of electrons is defined as:

$$\dot{n}_i = n_i p V_{eff} \left(1 - \frac{\eta}{\alpha}\right) \tag{2.6}$$

Where p is pressure, V_{eff} is the volume which is exposed to the electric field (and/or radiation) and n_{irad} is:

$$n_{irad} = C_{rad} \Phi_{rad} \left(\frac{\rho}{p}\right)_0 \tag{2.7}$$

The variable n_{irad} is the number of electrons present due to radiation. Coefficient, C_{rad} is a coefficient which characterizes the radiation - gas ionization process. The quantum flux density of the radiation is defined by Φ_{rad}, $\left(\frac{\rho}{p}\right)_0$ is the pressure reduced density of the gas.

Under conditions where surface emissions dominate the source of electrons can vary significantly. Electron emission can occur from the conductor surface due to radiation or electrons can be trapped in defects along the surface of the insulator or electrons can be emitted due to impact ionization or due to photo-ionization. The surface emission process can be closely approximated by the Richardson-Schottky emission equation:

$$\dot{n}_e = \frac{A}{e} S e^{-\left[\frac{\Phi - \sqrt{\frac{e^- E}{4\pi\epsilon_o}}}{kT}\right]} \left(1 - \frac{\eta}{\alpha}\right) \tag{2.8}$$

In this case e^- is the charge of an electron, ϕ is a work function which describes the energy required for a given material to emit an electron. E is the electric field at the emitting surface, k is the Boltzman constant, T is the temperature and S characterizes the surface material properties. If a defect is present in the bulk of a material or ionization takes place far from a conducting or semi conductive surface volume generation will be the dominant source of seed electrons. If discharges take place near a conductor then surface ionization will play a significant role.

2.2.2 Mean Free Path of Electrons

A key factor in understanding the relation of the Townsend mechanism to gas properties is the mean free path of electrons, λ_m. Where λ_m is the average distance between molecules (or atoms) in a gas and will

depend on both the atomic size of the molecule and the pressure of the gas (assuming a constant volume scenario). The Townsend mechanism is based on collision ionization of electrons, and it is important to classify the two types of mechanical collisions possible. First, elastic collisions which preserve the kinetic energy of the objects both before and after collision. Second is inelastic collisions in which the kinetic energy will change forms (thermal, electromagnetic through absorption, or ionization) as a result of the collision. In an electric field electrons are accelerated, and concurrently the electron collides with a molecule in an elastic collision the electron will change direction but maintain its velocity and continue to accelerate. In this case the electron will continue to gain energy and will eventually gain enough kinetic energy to ionize a molecule by the collision. In the same collision scenario modified such that collisions between the electron and the molecule are inelastic, some of the energy will be converted into another form meaning the electron will loose some velocity. If enough inelastic collisions occur, the electron in the same electric field may never gain enough velocity to ionize the molecules by impact ionization. The only way ionization could principally occur in that scenario would be to increase the rate of electron acceleration by increasing the electric field magnitude. In all gasses both elastic and inelastic modes of collision will be present, but the specific nature of the patterns will depend significantly on the gas itself. Also, note the concept of the mean free path of electrons is directly related to pressure, and the required field to breakdown will be proportional to the gas pressure. The direct analysis of the dependence on breakdown strength as a function of pressure is defined as Pachen's law [3, 16].

2.2.3 Pachen's Law

The coefficients relating to gas breakdown depend on the type of gas present. To provide examples for the coefficients used two of the most common dielectric gases, air and Sulfur Hexafloride (SF6), bwill be considered with approximate breakdown strength under atmospheric pressure in Table 2.1 . In a majority of applications what is of interest is the ability of a gas to withstand a voltage without breaking down. Pachen's law is what allows for the breakdown strength in volts or kV/mm to be calculated.

Table 2.1: Breakdown Strength of Air and SF6 Under Atmospheric Conditions

Material	Relative Permittivity	Breakdown Strength-1bar [kV/mm]
Air	1.00	3
SF6	1.00	9

The breakdown strength of both air and SF6 is highly dependent on the pressure and distance between conductors, and for air the dependence on pressure is given by Paschen's Law with the relevant parameter

values of Table 2.2 and assuming a uniform electric field is given by:

$$V_{breakdown} = \frac{B \cdot p \cdot d}{ln(A) - ln[ln(1 + \frac{1}{\gamma_{se}})] + ln(p \cdot d)} \tag{2.9}$$

This equation can be approximated for sufficiently large values $p \cdot d$ (as long as the value is not in the low pressure/low distance paradigm).

Table 2.2: Paschen's Law Parameters

Material Properties		
Parameter	Value	Description
B	39 $\frac{V}{kPa\dot{c}m}$	Experimentally Obtained Gas Constant
d	>0 [m]	Distance
A	0.95 $\frac{1}{kPa\dot{c}m}$	Experimentally Obtained Gas Constant
p	>0 [Pa]	Pressure
γ_{se}	1	Secondary Electron Emission Coefficient

The impact of pressure on breakdown voltage is seen graphically in Figure 2.1 which shows that at high pressures and very low pressures the breakdown strengths increase. The reason for the increase in breakdown strength at low pressures is because there are simply not enough gas atoms to be ionized as a vacuum condition is approached.

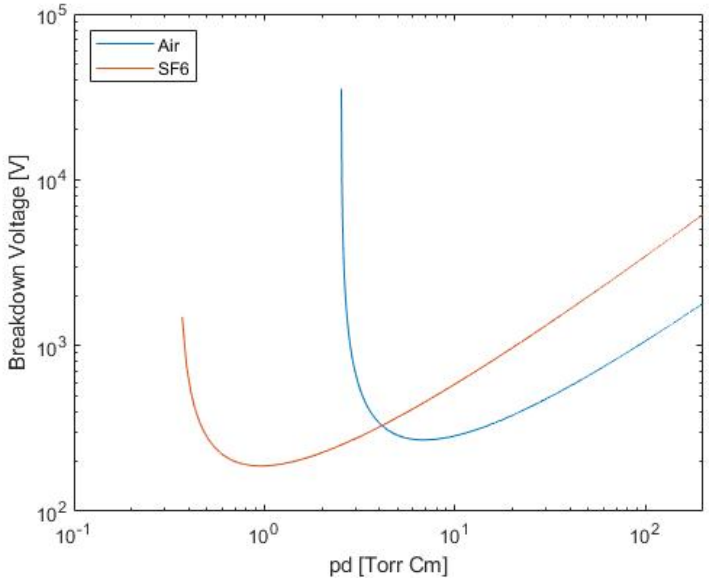

Figure 2.1: Breakdown Strength vs. Pressure for Air and SF6

It is observed that at higher values of $p \cdot d$, both air and SF6 have larger breakdown strengths. This is in

large part due to the high electron affinity of SF6 which is the ability of a molecule to capture electrons and exist as a quasi-stable negative ion. To be more specific electron affinity is measured as the amount of energy released from a molecule when an electron is captured. The more energy released the higher the electron affinity.

The Townsend mechanism transitions to streamer discharges when the product of $p \cdot d$ is large and specifically large enough if the number of electrons in an avalanche exceeds 10^6. In this case the electron avalanche produces its own electric field which can significantly amplify the initial electric field distribution. This field enhancement causes an increased amount of ionization collisions (which produce the avalanches) and recombinations (which emit photons). The emitted photons can produce secondary avalanches near to the end of the avalanche. This same process occurs in non-uniform fields which are much more commonly seen in power system applications.

2.2.4 Gas Discharges in Non-Uniform Fields

In non-uniform fields the ionization coefficient will depend on the electric field, $\alpha = \alpha(E)$. As a result the calculation of discharge inception voltage will depend on the geometry (as the geometry and voltage are the two things which determine the electric field). If the field is weakly non-uniform then in the region where the electric field is uniform the Townsend criteria and mechanism will approximately hold. But in the case of strongly non-uniform fields discharges can occur locally in the region of high electric field, based on similar concepts to the Townsend mechanism but slightly modified. In this case incepted discharges can not cause immediate breakdown as in the case of a uniform field, the discharges begin at a electrode, and if the field is increased can grow into streamer, which corresponds to discharges which move into the region of low electric field. Streamers can move into the region of low electric field because they are dominated by the space charge associated with an avalanche. At the head of the avalanche the number of electrons present grows, and so does the rate of ionization and recombination processes. Once the number of electrons in the front of the avalanche grows to about 10^8 electrons, the result of recombination effects begins to dominate. Recombination produces a photon which being electromagnetic radiation can be absorbed by atoms resulting in the excitation of electrons or if the photon has enough energy the ionization of the atom (photon energy is directly proportional to the frequency). If the photon causes ionization it is called photo-ionization. Photo-ionization can result in the formation of a new avalanche, even outside of the region of maximum background electric field (field in the absence of space charge or polarization effects). The requirement for streamer inception is given by Raether's ignition condition:

$$\int_0^d (\alpha - \eta) dx \geq N_{crit} = K_{st} \tag{2.10}$$

Where as in the case before alpha and eta are the ionization and recombination coefficients and N_{crit} is the critical number of electrons, and K_{st} is the streamer inception factor which is in general different than the Townsend ignition criteria parameter values. It is also important to note that if an insulator is present the surface of the insulator can have a significant impact on the ionization coefficients α and η [37].

2.3 Partial Discharge Theory

Partial discharges are defined as discharges which partially bridge the gap between electrodes and do not cause a complete breakdown. Partial discharges can be broken down into three categories. First is internal partial discharge which occurs in a air pocket in a bulk dielectric material. Second is surface discharge which is a gas discharge occurring along the surface of a solid dielectric. Third is corona discharge which is a gas discharges which occurs from an electrode in gas but does not cause a breakdown.

2.3.1 Internal Discharges

To understand internal discharge take the example of a parallel plate capacitor with a spherical void lying exactly in the middle of parallel plates. Internal defects can occur due to imperfections in the manufacturing process, delamination or mechanical vibration . If the electric field increases above a threshold gas discharge will incept in the cavity where the electron avalanche (plasma) will travel from the top of the cavity to the bottom. It is important to note that often dielectric materials are chosen with a relative permittivity greater than 1 (typically between 2 and 10). This means an air cavity will have a larger electric field relative to what is present in the solid dielectric under AC electric stresses. An example of a defect in which partial discharge could be incepted is shown in Figure 2.2. This is just one type of defect which could be present, a wide variety of defect geometries can be present [5].

Assuming a spherical cavity (or approximately for a flat cavity) of height d, the partial discharge inception field was derived by Niemeyer [37].:

$$\int_0^d \bar{\alpha}[E(x)] dx \geq K_{st} \tag{2.11}$$

E(x) is the electric field along the streamer path, K_{st} is the number of electrons which must accumulate along the avalanche head which produces a large enough secondary electric field keeping the process sustaining, $\bar{\alpha}$ is the effective ionization coefficient. Upon solution of this integral the following relation is obtained in of

the electric field required for inception as a function of pressure, defect height and gas parameters.

$$E_{inc} = \left(\frac{E}{p}\right)_{cr} p\left(1 + \frac{b}{(dp)^{\frac{1}{\beta}}}\right) \tag{2.12}$$

Where b is a gas constant defined as:

$$b = \frac{(K_{cr}/C)^{1/\beta}}{(E/p)_{cr}} \tag{2.13}$$

Where $\left(\frac{E}{p}\right)_{cr}\left[\frac{kV}{mm \cdot bar}\right]$ is the pressure reduced critical electric field. The constants C and β (which is 2 for air) are parameters which correspond to the steepness of the effective ionization coefficient once E_{cr} is exceeded[37]. These parameters have been found experimentally, solving for b it holds as a gas constant describing the effective rate of ionization of a gas with a value of 8.6 for air. As previously mentioned partial discharge inception has a large pressure dependence p in Pa, and d is the cavity height in meters. The parameter values can change depending on the gas present as well. If there are different material interfaces present with several potential examples shown in Table 2.3. In addition to providing a way to define an inception field for a spherical defect geometry several qualitative observations are apparent. First as in the case of Pachen's law at large values of pressure the inception field becomes large, and at low pressures the inception field is small (unless the pressure is very near to a vacuum condition). Second the inception field decreases as the size of a cavity increases.

Table 2.3: Values of Model Parameters Used in the Gas Discharge Equation

Gas/Surface	$\left(\frac{E}{p}\right)_{cr}\left[\frac{V}{Pa \cdot m}\right]$	β	C $[Pa^{\beta-1} \cdot m^{beta-1} \cdot V^{-\beta}]$	K_{cr}
Air	25	2	4.15×10^{-4}	9
Air/PVC	≈25	≈2	$\approx 4 \times 10^{-4}$	≈9
Air/Glass	≈25	≈2	$\approx 4 \times 10^{-4}$	≈9
SF_6	89	1	2.8×10^{-2}	10.5

Calculation of the partial discharge inception voltage can be found analytically for any ellipsoidal cavity. The inception voltage can also be calculated by Finite Element Methods, and holds approximately even for non-ellipsoidal cavities. Analytically the inception voltage is found by solving the integral.

$$V_{inc} = \int_{x'=h}^{x'=0} \frac{E_{inc}}{f} dx \tag{2.14}$$

Where f is a geometric factor which accounts for local field enhancement and will depend on the geometry of the cavity defined as:

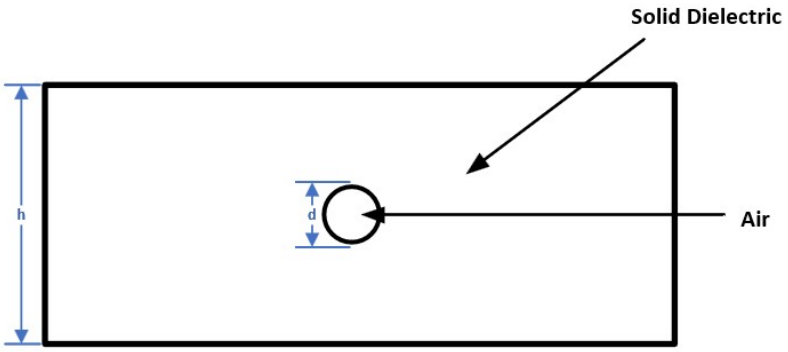

Figure 2.2: Air Cavity in the Bulk of a Dielectric

$$f = \frac{K\left(\frac{a}{b}\right)\epsilon_r}{1 + \left[K\left(\frac{a}{b}\right)\right]\epsilon_r} \tag{2.15}$$

Where a is the horizontal radius of the ellipsoid, and b is the vertical radius of the ellipsoid, and ϵ_r is the dielectric relative permittivity [9]. For an oblate ellipsoid K is defined as:

$$K\left(\frac{a}{b}\right)_{oblate} = \frac{\left(\sqrt{\left(\frac{a}{b}\right)^2 - 1}\right)^3}{\left(1 + \left(\sqrt{\left(\frac{b}{a}\right)^2 - 1}\right)^2\right)\left(\sqrt{\left(\frac{b}{a}\right)^2 - 1} - tan^{-1}\left(\sqrt{\left(\frac{b}{a}\right)^2 - 1}\right)\right)} \tag{2.16}$$

And for a Prolate ellipsoid K is defined as:

$$K\left(\frac{a}{b}\right)_{prolate} = \frac{2\left(1 - \sqrt{1 - \left(\frac{b}{a}\right)^2}\right)^3}{\left(1 - \left(\sqrt{1 - \left(\frac{b}{a}\right)^2}\right)^2\right)\left(ln\left(\frac{1+\sqrt{1-\left(\frac{b}{a}\right)^2}}{1-\sqrt{1-\left(\frac{b}{a}\right)^2}}\right) - 2\sqrt{1 - \left(\frac{b}{a}\right)^2}\right)} \tag{2.17}$$

These equations provide a formulation for the calculation of the partial discharge inception field and voltage for any ellipsoidal cavity. For the case of internal discharge it is often difficult to predict in the design stage as the cavities in which they occur are a product of a defect either during the insulation life or during manufacturing. If internal discharge is incepted during the life of an electrical asset it can result in a significant reduction of life and can lead to failure. The damage as a result of a partial discharge will approximately depend on the amount of charge which is transferred during the partial discharge event, i.e. discharge magnitude in C, or mV [20]. An example of a typical phase resolved partial discharge pattern for an internal cavity is shown in Figure 2.3.

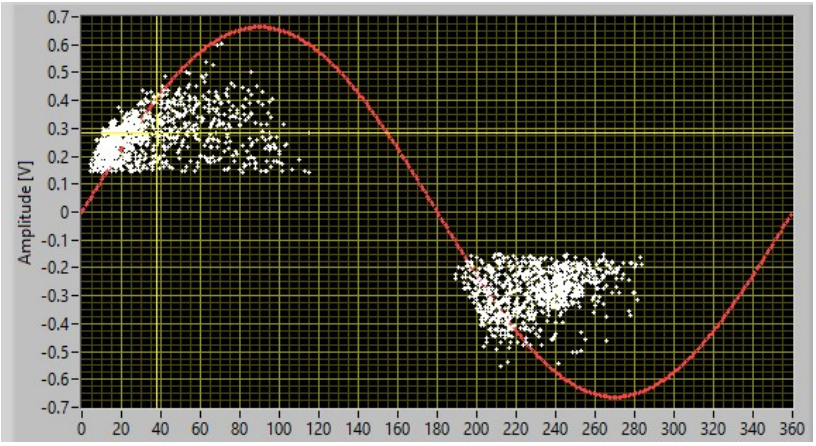

Figure 2.3: Phase Resolved Partial Discharge Pattern of Internal Partial Discharge

2.3.2 Surface Discharges

Surface discharges occur along the surface of an insulator and typically originate at a triple point (the interface between air, solid insulation and a conductor). Surface discharges can either be a local discharge or bridge the gap between the conductors in a flashover. Surface flashover is accounted for in insulation design by the creepage distance between electrical terminals (and/or ground) across the surface of the solid insulation [23]. Creepage distance however provides little insight into the local surface discharge inception voltage which will be heavily dependant on the electric field near the triple point. Two prototypical examples of different triple points are shown in Figure 2.4. Discharges which are local to the triple point are often categorized as glow discharge, and if the field is increased (not so high as to cause a flashover) such that the discharges begin to travel a longer distance (in particular into the region of lower electric field) the surface discharges are categorized as streamers.

A surface discharge model has also recently been proposed which takes the same form as the gas discharge model for internal cavities with different coefficients and an additional parameter: [36].

$$E_{inc} = \left(\frac{E}{p}\right)_{cr} p \left(\frac{b}{(pk_s l)^{\frac{1}{\beta}}}\right) \tag{2.18}$$

In air the coefficients take the following values, $\left(\frac{E}{p}\right)_{cr}$ is 8 $\frac{V}{Pa \cdot m}$, β is 2, b is defined the same as before but will take a different value as the dielectric surface can contribute to the avalanche process. As a result the value of C is taken to be 7.6×10^3 which results in a value of b equal to 4.3. In addition the value of d which was previously defined as the cavity height becomes l, and this is the creepage distance [m] along the shortest path between terminals (or from terminal to ground). The product of k_s and l can be thought of as the distance where the electric field is constant and maximum as in the case of gas discharge [36]. The

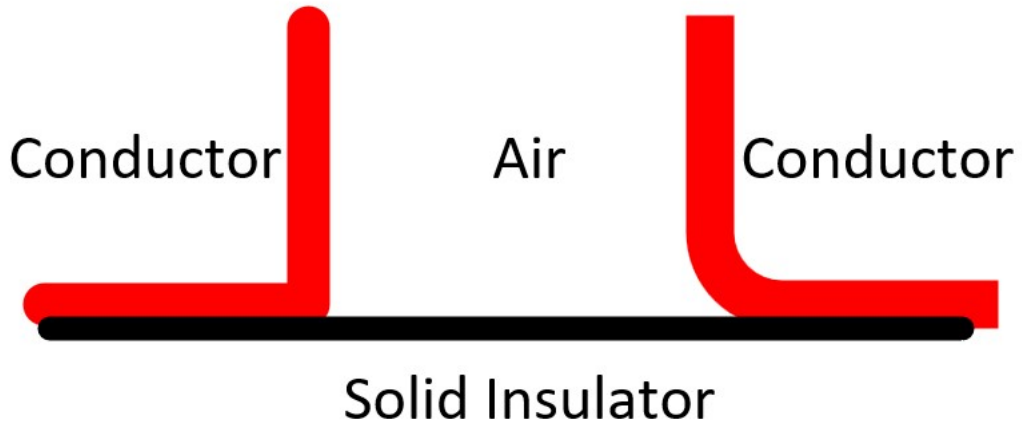

Figure 2.4: Electric Field Triple Points

new parameter k_s is determined by the field profile present and has two definitions, first for monotonically decreasing fields:

$$k_s = \frac{l(0.95E_{max}^{Tan}) - l(0.8E_{max}^{Tan})}{l} \tag{2.19}$$

For fields which are not monotone (i.e. have regions where the field increases to reach a maximum then begins to decrease).

$$k_s = \frac{l(0.95E_{max}^{Tan})^{+} - l(0.95E_{max}^{Tan})^{-}}{l} \tag{2.20}$$

Where E_{max} is defined as the maximum electric field, l is the total creepage distance and $l(x)$ is the distance at which the specified electric field is located. In the case of a uniform electric field, $k_s = 1$ as in the case of partial discharge in an internal cavity. Note to complete the calculation of the surface discharge inception voltage an electric field profile is required. This can be found through finite element analysis using tools such as COMSOL. Variable k_s has a geometric interpretation which can be seen for both cases in Figure 2.5. Surface discharges can result in surface erosion, pitting and eventual failure of an electrical insulation system. Surface discharges while not as severe as internal partial discharges can result in a significant degradation of insulation system life. For surface discharge one factor which can have a significant influence on the inception field and voltage is surface pollution. Many different environmental factors can change the electric field distribution and increase the likelihood of surface discharges or flashover. Some of which include water condensation, dust/sand, conductive or semi-conductive particles and salt to name just a few. Some materials are resistant to pollution flashovers. For example porcelain, glazes or glass are not permanently effected by surface discharges, however organic insulators can erode and quickly degrade as a result of surface

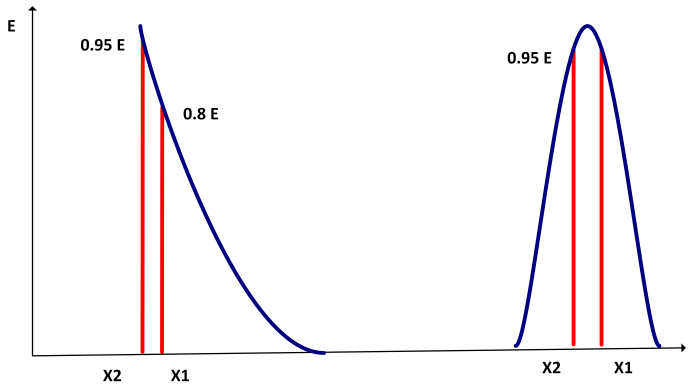

Figure 2.5: Electric Field Profile Types

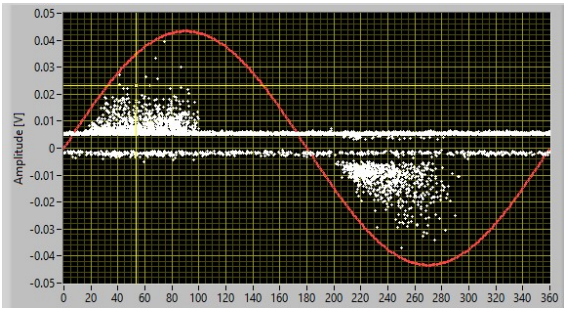

Figure 2.6: Phase Resolved Partial Discharge of Surface Discharge

discharges and are much more susceptible to pollution driven discharge. An example of a surface discharge phase resolved partial discharge pattern is shown in Figure 2.6

2.3.3 Corona Discharges

To briefly summarize internal discharges occur in air pockets in a bulk solid dielectric material, surface discharges occur along the surface of an insulator as a result of the triple point. Corona discharge is a gas discharge which occurs from an electrode into a gas. Corona discharge is different from the previous two types of discharge as it does not occur with relation to a solid dielectric. Corona discharge can only occur in non-uniform electric fields (and typically only occurs in highly non-uniform electric fields), and as a result the inception condition is given by Raether's ignition condition. Corona discharge at or above the inception criteria will produce local avalanches which will be dominated by collision ionization and will produce ionization very near to the electrode. This type of discharge is called glow corona. At higher fields streamer corona can form, and if the field becomes high enough a direct flash over can occur [7].
Corona discharges have the lowest impact on insulation aging compared to internal partial discharges or surface discharges. Nevertheless corona can drive dielectric losses in a power system, and can produce gas bi-products that may deposit on the surface of insulation (causing pollution), and produce toxic gases.

2.3.4 Partial Discharge under AC and DC Voltages

Under AC conditions the electric field is driven predominantly by the relative permittivity of the dielectrics present. While under DC conditions the electric field is driven by the materials conductivity. In addition under AC conditions the electric field is time varying, the impacts of the differences between AC and DC result in differences in partial discharge characteristics. The first differences relates to the measurement of partial discharge, under AC partial discharge is generally observed by a phase resolved partial discharge pattern. This pattern correlates a partial discharge event (measured in pico-coulombs or mV) to the voltage phase in which the partial discharge event happened. Under DC conditions there is no phase relation to a partial discharge pulse, and consequently the partial discharge pattern is time resolved. In both AC and DC there is a stochastic lag (statistical time delay) between the applied voltage and the inception of partial discharge due to the availability (or lack of availability) of a seed electron which initiates the avalanche process[12]. Once a partial discharge event occurs the electric field temporarily changes due to the charge displacement. Under AC conditions the time varying fields quickly recover to the field distribution because the voltage is time varying allowing for another discharge to follow the first. Under DC conditions after a partial discharge it takes time for the electric field to return to its nominal condition resulting in a longer delay between partial discharges. This time period between pulses is defined as the repetition rate with units of $\frac{pulses}{s}$. It is also important to note that partial discharges extinction is lower than the inception voltage, so partial discharge can continue even if the voltage has decreased to below the inception voltage.

2.4 Solid Dielectric Breakdown Theory

The three main sources of dielectric breakdown are electrical, thermal and mechanical. Each of which results in complete material failure. Electric breakdown of a solid dielectric is similar to the case of air. When the electric field exceeds a threshold which depends on the specific material the insulation will fail resulting in conduction. Thermal breakdown occurs if the temperature of the dielectric becomes large enough and can produce macroscopic damage to the material. Mechanical breakdown occurs if the mechanical stress (either tensile or compression) leads to a mechanical fracture of the dielectric. Each of these failure modes can also combine to result in failure of an insulation system at a net lower individual stress level.

2.4.1 Weibull Distribution

A powerful tool for experimental analysis which is commonly used for breakdown testing is the Weibull Distribution which is an extreme value distribution,

$$F(s) = 1 - e^{-(\frac{s}{\alpha})^{\beta}} \tag{2.21}$$

Variable α is the scale parameter, β is the shape parameter and s is the measured parameter.

2.4.2 Electrical Breakdown

The breakdown of solid dielectric materials is best described by solid state theory. Solid state theory explores the impact of atomic scale properties on macroscopic properties and vice versa. A first observation is the differences between conductors and insulators. In a conductor there are continuous allowed energy levels between the valence band and the conducting band making the required energy between transitions from valance to conducting small. In the case of an insulator there is a forbidden region of energy between the valance and the conducting band. A forbidden region corresponds to a region of energy of which electrons cannot take (classically forbidden). Typically these relationships are shown graphically by a band diagram.

In a solid dielectric transitions occur between the valance and the conducting band when a sufficiently high electric field is applied to the lattice which allows for the electrons to "tunnel" through the forbidden region into the conducting band. It is important to note that for this breakdown to occur in an ideal crystal dielectric the required field is extremely high, much higher that what is observed experimentally. This is due to the presence of imperfections in every material (trapped particles, grain boundaries etc.) which appear as additional states in the forbidden region. It is the presence of these defects that lower the breakdown strength as the required electric field to move electrons from the trapped defects into the conduction region is lower. Once a sufficient number of electrons move into the conduction band of the dielectric it will conduct and fail. In practical applications as the size of an insulation system increases so do the number of defects that are present. Thus at higher volumes the lower volumetric electric strength (kV/mm) due to the presence of more defects. The behavior of these trapped states will be explored in much more depth in the section on Conduction Mechanisms of Dielectrics.

2.4.3 Thermal Breakdown

Thermal breakdown of a dielectric material occurs if the amount of heat which is put into the dielectric is greater than the amount of heat removed. This is important to note because dielectrics in general have a low thermal conductivity and can also often have a large thermal capacitance (note thermal capacitance only arises in transient conditions). If we take the case of a medium voltage cable, as the cable heats up due to ohmic losses and there is a dielectric material between the conductor and the ambient air. An unstable condition can occur where the heat removed occurs at a rate lower than the heat is supplied this imbalance

will eventually result in material failure. In the steady state of a cable the heat applied must be equal to the heat removed. This balance equation is defined as:

$$P_{supplied} = P_{dissipated} \tag{2.22}$$

Note a second condition must be also considered during thermal transients because of the associated thermal capacitance. This additional boundary condition is that the rate of change of the heat must also be the same. If the rate of change of the source heat is larger than the rate of change of the heat dissipated, and above a threshold, the dielectric material will also breakdown. One factor which also can significantly decrease the heat removed from the conductor is the dissipation factor, $tan(\delta)$, which defines that the losses in the insulation system. This allows the supplied heat to be broken into two terms:

$$P_{supplied} = P_{ohmic} + P_{\delta} < P_{limmit} \tag{2.23}$$

The last aspect to thermal breakdown is the concept of a thermal threshold which is the temperature at which the dielectric will breakdown. If either of the two equations above are violated (more heat is put into the insulator than removed) but the temperature threshold is not exceeded there will not be a thermal breakdown. The thermal breakdown of dielectrics can also be related back to band theory as the probability of an electron tunneling to the conduction band is a function of temperature. As the temperature increases the required electric field for breakdown will decrease. If an electron is present in the conduction band it is free to move through the lattice structure.

2.5 Charge Transport

Charges can be transported in a material by several different mechanisms with the underlying assumption of solid state physics. To be precise band theory does not hold in polymeric insulation systems as polymers are amorphous and not crystalline (which is the assumption of solid state physics). Nevertheless the solid state approach can provide some valuable insights into the behavior of solid insulation systems. Under band theory electrical insulators have a large band gap. Which would require a significant electric field before electrons have enough energy to tunnel to the conduction band. In fact the phenomena of breakdown shows that the behavior of dielectric breakdown does not exactly follow this response. As the measured breakdown values are much lower than what would be predicted by the materials band gap. This means that there are additional processes at play. One of these additional dominant modes is caused by traps which are energy states in between the valence and conduction band. These concepts are represented graphically in Figure

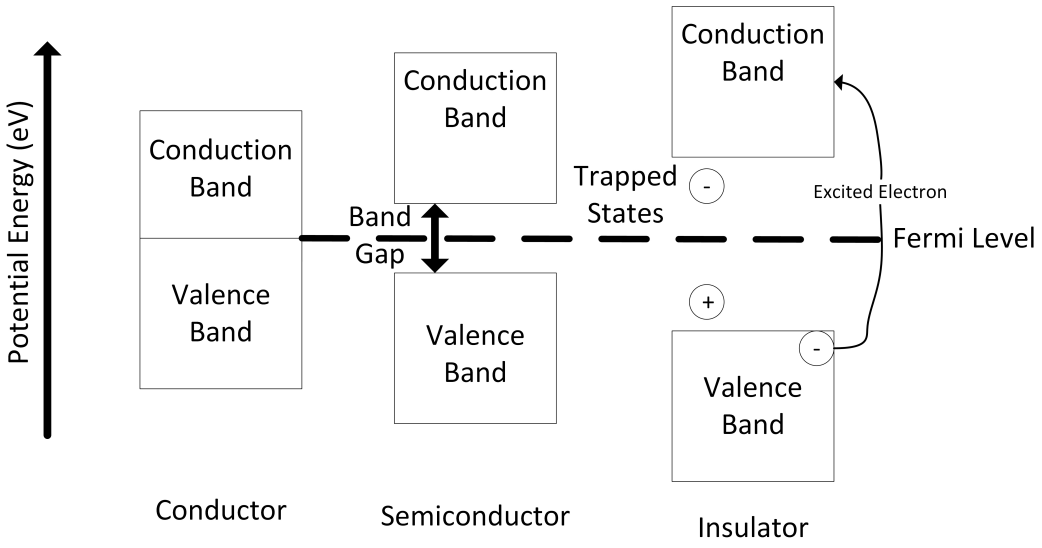

Figure 2.7: Solid State Band Theory

2.7.

Trap states for electrons or holes correspond to lattice defects of which the specific energy level would be forbidden in a perfect crystalline structure. As is the case for air electrons have a much higher mobility compared to holes in part due to their smaller mass. Defects can "donate" an electron and become holes allowing for an electron which is present in the valence band to tunnel to the conducting band. While these holes are not mobile they can still interact with the mobile electrons causing neutralization. For dielectrics purely electrical effects are not sufficient to explain the conduction phenomena as a result several additional fundamental mechanisms are introduced. While a variety of electron transport mechanisms are possible, they can be categorized in two ways. First by mechanisms which are dominated by the interface of the dielectric with a conductor. Second mechanisms which are dominated by the dielectric bulk [46].

2.5.1 Interface Dominated Conduction Mechanisms

The first interface dominated conduction mechanism which was previously discussed is Schottkey emission. This conduction mechanism plays an important role in modeling of gas discharges. Schottkey or thermoionic emission is the dominant interface dominated process at sufficiently high temperatures (near roomn temperature), but is unable to describe the emission process at low temperatures which results in the introduction of a second emission process.

Fowler-Nordheim Tunneling

Fowler-Nordheim Tunneling occurs if the electric field is high enough at the surface of a conductor such

that an electron will tunnel from the conductor into the conduction band of the dielectric. The potential barrier at the interface of a conductor and an insulator is taken as a triangular barrier allowing for a solution to the Schrodinger equation. This tunneling is given by the equation:

$$J = \frac{q^3 E^2}{8\pi h q \phi_b} e^{\frac{-8\pi\sqrt{(2qm_T^*)}}{3hE}\phi^{3/2}} \tag{2.24}$$

Variable J is the current density, q is the elementary charge of an electron, E is the electric field, h is Planck's constant. The parameter ϕ_B is a work function which describes the potential at the conductor electron interface, and finally m_T^* is the tunneling effective mass of the electron. Tunneling will dominate electron emission at the interface of a conductor and an insulator at sufficiently high electic fields. Note Schotkey and Fowler-Nordheim are the tprimary interface dominated conduction mechanisms, while others exist these are the two most relevant for this review.

2.5.2 Bulk Dominated Conduction Mechanisms

Bulk dominated conduction will depend primarily on the trap energy levels present. In other words relating to the amount of defects present as well as relating to the natural amorphous material properties in the case of polymeric insulation.

Ohmic Conduction

Ohmic conduction is the most well known type of conduction as it provides a linear model between the current density and the electric field in the form of:

$$J = \sigma E \tag{2.25}$$

The constant σ is the materials conductivity, J is the current density and E is the electric field in the material. Ohmic conduction occurs as a result of electrons which are present in the conduction band that can freely move when an external electric field is applied to the material. In the case of a dielectric material the amount of electrons in the conduction band are initially very small. The conduction mechanisms in dielectrics ohmic conduction can only be observed at very low fields. As at high fields other mechanisms of electron transport will dominate, producing a non-linear conduction characteristic.

Poole-Frenkel Emission

Poole-Frenkel Emission is comparable to Schottkey emission located in the bulk of a dielectric where

upon the application of an electric field the effective potential barier seen by an electron (or a hole) in a trap state is decreased. As a result of the decrease in the effective trap depth the probability that the electron is thermally excited into the conduction band increases. The governing equation for Poole-Frenkel emission is:

$$J = q\mu N_C E e^{\frac{-1(\phi_T - \sqrt{qE}/\pi\epsilon_i\epsilon_0)}{kT}} \tag{2.26}$$

Variable μ is the electronic drift mobility, N_C is the density of states in the conduction band and ϕ_T is the trap energy level. Poole Frankel emission is found to dominate at sufficiently large temperatures and electric fields

Hopping Conduction

Hopping conduction occurs when electrons tunnel between trapped states as a result of thermal excitation. The expression of hopping conduction is:

$$J = qanve^{\frac{qaE - E_a}{kT}} \tag{2.27}$$

Variable a is the distance between trap states, n is the electron concentration of the conduction band, v is the thermal vibration in the trap states, and E_a is the electron activation energy. Hopping transport occurs at sufficiently high temperatures and low electric fields.

Space-Charge-Limited Conduction

Space-Charge-Limited conduction occurs when the amount of electrons injected into a dielectric becomes sufficient to fill all trapped states. When the electron is injected into the dielectric from a conductor it will be in the conduction band and due to thermal relaxation can move into trap states. If the electron generation mechanism becomes large enough (at sufficiently very high electric fields) all of these trapped states will be full, and the electrons will remain in the conduction band resulting in a large increase in current once the process has initiated. At this point the electric field can no longer be assumed to be uniform as the trapped states will result in a new charge distribution which will limit the conduction [5, 4].

2.6 Space Charge

Space charge theory describes the distribution of charged particles in a material's bulk volume, along a material's surface or in a gas typically when an electric field is present. Because charged particles exposed to an electric field will experience a force which in gasses result in charge movement. In solids the movement of

ions can occur if the electric field is large enough to cause electron injection. In either case the introduction of space charge will result in a reduction of the global electric field (but can cause local field enhancements). In addition transient conditions can result in a significantly amplified electric field. As a result of this space charge plays a much larger role under DC conditions compared to AC. This is because under AC conditions the electric field is constantly changing which prevents the accumulation of space charge in a material bulk. However if partial discharge is present the space charge distribution can play a significant role when it comes to the partial discharge characteristics [39].

Under DC steady state conditions with no space charge or partial discharges the time rate of change of the electric field is zero. If space charges are introduced then a time varying component of the electric field would be introduced. One of the primary ways this occurs is as a result of partial discharges which is fundamentally a movement of charge. As a consequence of a partial discharge event a charge distribution is formed along a dielectric surface or in the bulk off the dielectric. Partial discharge is not the only mechanism which will change the charge distribution. Even if a discharge does not occur space charge can accumulate in the bulk of a specimen or along the surface over time due to an electric field[17, 21].

Under AC partial discharges the space charge can play a significant role when considering the "memory effect". The memory effect is the physics which explains variations of partial discharge measurements as a direct consequence of the partial discharge activity. The explanation of this effect will depend on the geometry present, mainly the type of discharge (Internal, Surface, or Corona). Once a partial discharge event occurs a transfer of charged particles are transferred to either end of the cavity (depending on the polarity). These moved charges will result in a net electric field in the cavity which is different from that the initial field distribution. Under AC the increase and voltage quickly causes the electric field to begin to increase even after a partial discharge event. Under DC the charges will begin to relax through drift diffusion and recombination events slowly over time. Under AC however the impact of this charge accumulation has a significant impact on the phase resolved partial discharge pattern, mainly the phase angle where inception begins. This phenomena allows for methods of defect identification based on the differences in phase resolved partial discharge patterns relating it to the type of partial discharge present.

2.7 Life Modeling of Electrical Insulation Systems

The aforementioned electrical, thermal and mechanical factors which can cause dielectric failure can also cause premature aging over a much slower time period (bus still shorter than the design life). Capturing these aging mechanisms into a model which is able to estimate the life of the insulation system has been the subject of much research. Several of these models have been proposed depending on the type of stress

present. First is the Dakin model for electrical stress, second is the general inverse power model, and finally the Eyring model for thermal stresses [12]. Each of these models are derived in two main steps, first by applying stress levels (electrical, thermal, etc.) until failure. The second step is repeat the test for multiple values of stress with the parameters fit by a recursive algorithm for the following models:

$$L = C_E e^{\left(\frac{-nE}{E-E_t}\right)} \tag{2.28}$$

$$L = C_E E^{-n} \tag{2.29}$$

$$L = C_E \left(\frac{h}{kT}\right) e^{\left(\frac{\Delta G}{kT}\right)} \tag{2.30}$$

Where L is the insulation life, C_E is a model coefficient, n is the voltage endurance coefficient, both of which will depend on material, electric field and temperature. The parameters k and n are the Boltzmann and Plank constants, with E and T as the electric field and temperature respectively. The constant ΔG is the Gibbs free energy of the electro-thermal degradation process. To combine the effect of thermal and electrical stresses additional parameters have been introduced by [30, 22]:

$$L = C_E T^w \left(\frac{h}{kT}\right) e^{\left(\frac{\Delta G}{kT}\right)} e^{\left(\frac{-(K_1+K_2}{T}\right)E} \tag{2.31}$$

With, k_1 and k_2 being additional coefficients, each of these models have parameters which must be found experimentally for a given material and application. The testing required to find these parameters often requires testing at multiple electric fields and temperatures. As the stress level decreases the life increases exponentially which often results in a prolonged testing time. The advantage of this method is once a life model has been found an empirical relation to estimate the life of an insulation system based on the design stress can be found.

2.8 Automatic Partial Discharge Software

Much work has been done by Montanari et. al. on the development of innovative automatic partial discharge software which is able to *Separate* recorded pulses, *Recognize* noise and partial discharge pulses, and *Identify* (for the latter) of the type of partial discharge, internal, surface or corona. The final step in the process is the use of the partial discharge classification and time evolution in the production of diagnostic tools. These four concepts have been combined into the acronym *(SRID)*. [14, 15, 13]

2.8.1 Separation

Separation is fundamentally based on feature extraction of measured partial discharge pulses (in addition to noise which is always present). Several different methods for feature extraction have been proposed which include the Fast Fourier Transform (FFT), principal component analysis (PCA), Neural Networks, support vector machines (SVM) or multi-dimensional mapping to name just a few. In the case of partial discharge Time-Frequency mapping is a common technique. Time-Frequency mapping plots a pulse with respect to its frequency component and pulse width (time). Because each of the partial discharge pulses may have an overlap with noise any mapping should include more than just frequency components and pulse width, this requires higher dimensional mapping and a projection into a 2D principal component space. For example if the partial discharge pulse and the noise have a similar frequency component, the time (duration) of the pulse would correspond to a second axis of which separation is more likely possible due to this increase in dimension. But it is also possible that in the Time-Frequency map overlap will occur due to coupling between the noise and partial discharge making automatic separation impossible. The first step in the process of separation is identifying the characteristics of each of partial discharge pulses which include (but is not limited to) the pulse amplitude, kurtosis, and skewness. By adding these features into a multidimensional space (which includes Time-Frequency characteristics) will in general will increase the probability that a 2 dimensional projection of the data can be separated. To find the two dimensional projection principal component analysis is used to locatte the most important features of the data acquired [32, 6].

2.8.2 Recognition

Once clusters of data are separated it is possible that multiple clusters of partial discharge and or noise are present. It is not possible to know how many clusters which are present until after the principal component analysis, Recognition is tasked with providing the distinction of the clusters present. The first approach to define the clusters is based on the average linkage algorithm:

$$d(a,b) = \frac{1}{n_a n_b} \sum_{i=1}^{n_a} \sum_{j=1}^{n_b} \sqrt{x_{ai}^2 + x_{bj}^2} \tag{2.32}$$

Where d is the average distance between clusters a and b,n_a and n_b are the number of members in clusters a and b. Variables x_{ai} and x_{bj} are the individual objects in the clusters and distance. It is still possible for over clustering as a result a cutoff threshold has been proposed.

Once clusters have been separated from each other rules are employed in determination of a given cluster is noise or partial discharge, One approach to this is the application of the weibull distribution of the signal

amplitude. In the case of partial discharge amplitude the measured data should fit well to the Weibull distribution but noise being random will not have a sufficient fit producing a large error. This can be found by the correlation coefficient of the distribution.

2.8.3 Identification

Identification is primarily concerned with determining the type and source of the partial discharge present. In the earlier case of recognition the Weibull distribution was used by Montanari et. al. to differentiate noise and partial discharge. The Weibull distribution can also be used as a metric in determining the type of partial discharge through the shape parameter β which for values between 1 and 2 signal surface discharge, values of around 10 signaling corona and values in between signaling internal discharge. Additional metrics can be employed including pulse shape and the Weibull distribution of the repetition rate, inception and extinction phase to name a few. These parameters which provide a relation can be combined in a fuzzy membership function at which identification is done by a percent confidence level. (i.e. 90% surface partial discharge and 10% internal discharge.) These factors combined allow for real world applications of automatic partial discharge software which can provide partial discharge diagnosis without the aid of an expert [17, 38, 43, 44, 42]

.

2.8.4 Diagnostics

Once identification of the source of partial discharge has been established it can provide a mechanism for establishing diagnostic tools relating the partial discharge mechanism to external aging. The ultimate goal of diagnostic tools, in particular online measurements is to allow for condition based maintenance where maintenance actions are based on need as opposed to time passed or equipment failure. Knowing the type of partial discharge is essential in diagnosis and condition evaluation as the type of partial discharge present will determine the need for a maintenance action. In the case of internal partial discharge the risk of failure can be quite large for the insulation system, but in the case of corona the risk of failure would be small as well as the consequent aging. This factor allows for a relationship between partial discharge and health to be derived from online measurements using the partial discharge software [18, 33].

The algorithmic approach should also be compatible with existing methods used by asset managers including System Control and Data Acquisition (SCADA). The general approach for a health index can be based on assigning a value between 0 (failure) and 1 (no aging). Montanari et. al. [33] also has proposed a health index which can in general evaluate broad classes of aging markers. In general these measurements

can come from both offline and online measurements. Observations about the insulation system result in a score which can take values between 1 and 5. The quantity of the observation is defined by the marker not the impact. It is important to recognize that not all types of aging are the same and to account for this a weight is required for each type of marker. These two factors are combined into a weighted average vector:

$$W_{AVG,i,j} = \frac{\sum_k S_{i,j,k} \cdot W_{i,j,k}}{\sum_k W_{i,j,k}} \tag{2.33}$$

Often power equipment has multiple sub-components, each sub-component can monitored, and evaluated independently. Each sub component are accounted for and assigned as an index i, The index j characterizes the number of characteristics under observation (Partial Discharge, Thermography etc.). The index k corresponds to the specific measurement associated with the characteristic (i.e. internal partial discharge, surface partial discharge or corona). The score is defined as S which is the previously mentioned diagnostic evaluation based on aging. The specific definitions of S can vary significantly depending on what is observed, some examples could be $tan(\delta)$, PD Amplitude or repetition rate. Whatever the marker chosen its minimum value should be 1, and maximum value should be 5. Finally W is the associated weight for the type of aging, the vector W can be any value (but will typically be between 1 and 5) which marks the impact of the score. From this weighted average a reliability can be established for the sub-component:

$$R_{i,j} = 1 - \frac{W_{avg.i,j} - SC_{min,j}}{SC_{MAX,j} - SC_{min,j}} \tag{2.34}$$

Where R is the reliability, $SC_{MAX,j}$ and SC_{min}, are the maximum and minimum observed score values. The overall health index can then be defined as the product of the reliabilities for the sub component, and the reliability of the asset as a product of the sub component reliabilities.

$$R_{i,j} = \Pi_j R_{i,j} \tag{2.35}$$

$$HI = \Pi_i PR \tag{2.36}$$

At the point of commissioning an asset a life expectancy is calculated (e.g. 30 years). Depending on aging factors the actual life may be shorter than the design. Online measurements produce a percent value of the life remaining which can be converted into relation between the health index and the residual life. This is defined as the product of the defined health index and the design life as:

$$L_R = HI \cdot L_D \tag{2.37}$$

By combining the partial discharge software with this health index approach weights for internal partial discharge, surface partial discharge and corona could be 5, 3, and 1 respectively. This allows for the measured partial discharge via online measurements to be converted into a single metric for the evaluation of residual life of an electrical asset allowing for optimization of maintenance activities. This approach of online monitoring can be incorporated into design and maintenance approaches to mitigate the aging effects of partial discharge [32].

2.9 Other Partial Discharge Mitigation and Insulation Design Approaches

Several different approaches have also been explored in literature to either eliminate or mitigate the effects of partial discharge on electrical insulation systems. In electrical systems the insulation system is one of the most susceptible to premature aging as a result of thermal degradation or partial discharge. Thus, ensuring the insulation system will reach the design life is of paramount importance in the design stage. The dependence of the aging mechanism on the environmental conditions can make this step even more challenging (and often impossible) which is what motivates the online monitoring discussed above. Some of the approaches which aim to increase the insulation reliability are based on developments in the material sciences toward materials which have unique and high performance. The first category of these materials are partial discharge resistant materials, which are materials nano-structured to endure partial discharge with minimal depolymerization. The second class of materials which are used are called electrets (electrical analog of magnets) which are materials with an intrinsic electric field. Partial discharges are primarily driven by the electric field in the environment they are placed. Electrets producing an electric field if placed properly provide an opportunity to "cancel" the electric field thus effectively eliminating a potential source for partial discharge.

2.9.1 Corona Resistant Materials

Corona resistant materials are created by the nanostructuring of materials which is achieved by the introduction of a small wt% of a given additive (eg. silica or polymide 6) to a bulk polymer [45]. The addition of the nanoparticles can have several effects, first the nano-particles will change the atomic structure of the solid which will increase the performance. Also the nano-particle themselves tends to have greater endurance to partial discharge. The nano-particles being distributed throughout the bulk of a material will change the degradation mechanism of partial discharge through the bulk.

2.9.2 Electrets

Electrets are materials which either through polarization of dipoles present in the material or through embedded electric charge producing a net electric field. Electrets can either be caused by permanent polarization of a material or through a charge distribution. The application of electrets to insulation system was proposed by C. Park as a way to mitigate the effects of triple points as well as insulation defects which drive partial discharge [40, 41].

Chapter 3

Surface Discharge Modeling and Testing

3.1 Laminated Bus Bar Geometry

In this chapter a laminated bus bar will be simulated and tested for surface partial discharges. In general for a laminated bus bar partial discharge could arise in internal cavities due to delimitation which while possible is much less likely compared to surface discharge that can occur at terminal triple points [24]. The electric field which drives surface discharge is primarily determined by the bus terminal geometry and the type of voltage source (AC, DC, or Modulated AC). In pursuit of this characterization simulation of the electric field was completed using COMSOL. The resultant field profiles allow for the surface discharge inception electric field and voltage to be calculated through Equation 2.9. The laminated bus bar 3D layout is shown in Figure 3.1, as well as a numbering layout for layers and testing configuration shown in Figure 3.2. Due to the bus bar layout 4 of the 6 sets of terminals can be tested directly. Each of the terminals are similar in layout and geometry, with the key difference being a slight difference in the angle which produces the line of minimum distance.

Before simulation of the electric field, a test procedure and approach must be established. For the laminated bus bar 4 of the 6 terminal pairs can be tested for surface discharge. Even for the 2 terminal pairs which cannot be tested a symmetry argument can be made suggesting similar partial discharge inception voltages to the other terminals (added to the fact of similar partial discharge inception voltages expected between the tested terminals). To test surface discharge under AC high voltage is applied through a capacitive voltage divider to terminals 1, 2, 3, and 4 independently (with all other terminals grounded). At the ground a high frequency current transformer (HFCT) senses partial discharge pulses by sensing high frequency current pulses in the return conductor. The HFCT is connected to a partial discharge measurement instrument with

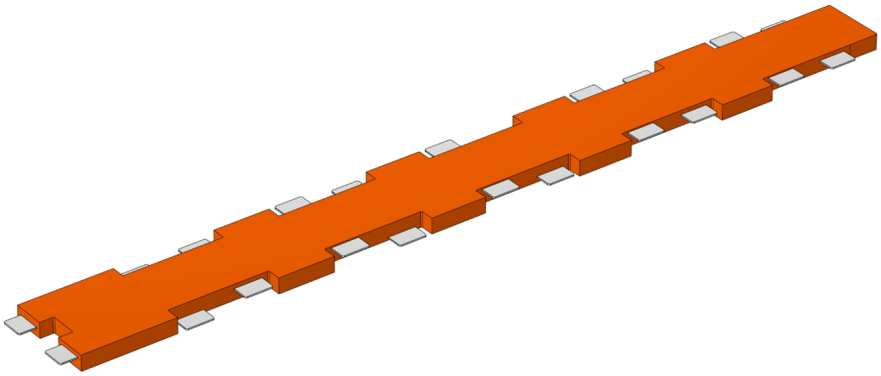

Figure 3.1: Laminated Bus Bar 3D

synchronization through a Rogowski coil. The partial discharge measurements are processed with the partial discharge software implemented by Montanari et al. There are two differences between the test set up when conducting DC PDIV tests compared to AC. First is simply the difference in the voltage generator under DC (and without the capacitive voltage divider) and second the lack of a synchronization signal. This test set up will determine which terminals are to be energized in simulations which allow for theoretical analysis.

Because electric fields between AC and DC are driven by different physical constants the partial discharge inception voltages can be significantly different. Laminated bus bars can be operated under modulated AC and DC conditions. Consequently, it is important that the insulation system is designed to avoid partial discharges under both scenarios.

3.2 Laminated Bus Bar under AC Operation

The laminated bus bar is insulated using an epoxy polymer resin (EPR) blend with a relative permittivity of 4. The primary risk of partial discharges occurs at the terminal, air insulation interface (triple point). The maximum electric field enhancement will occur in the region of the triple point with the shortest proximity to the ground electrode. The local field enhancement is first seen through simulation of the electric field norm shown in Figure 3.3. The field norm shows just how non-uniform the electric field. Appears a a significant field enhancement is observed in near proximity of the triple point, but in the middle of the terminals it is almost 0. The electric field norm provides the absolute value of the electric field, however surface discharge is driven by the tangential component of the electric field. The relation of the electric field to the surface discharge inception voltage can be found by application of the surface discharge model introduced in chapter 2.

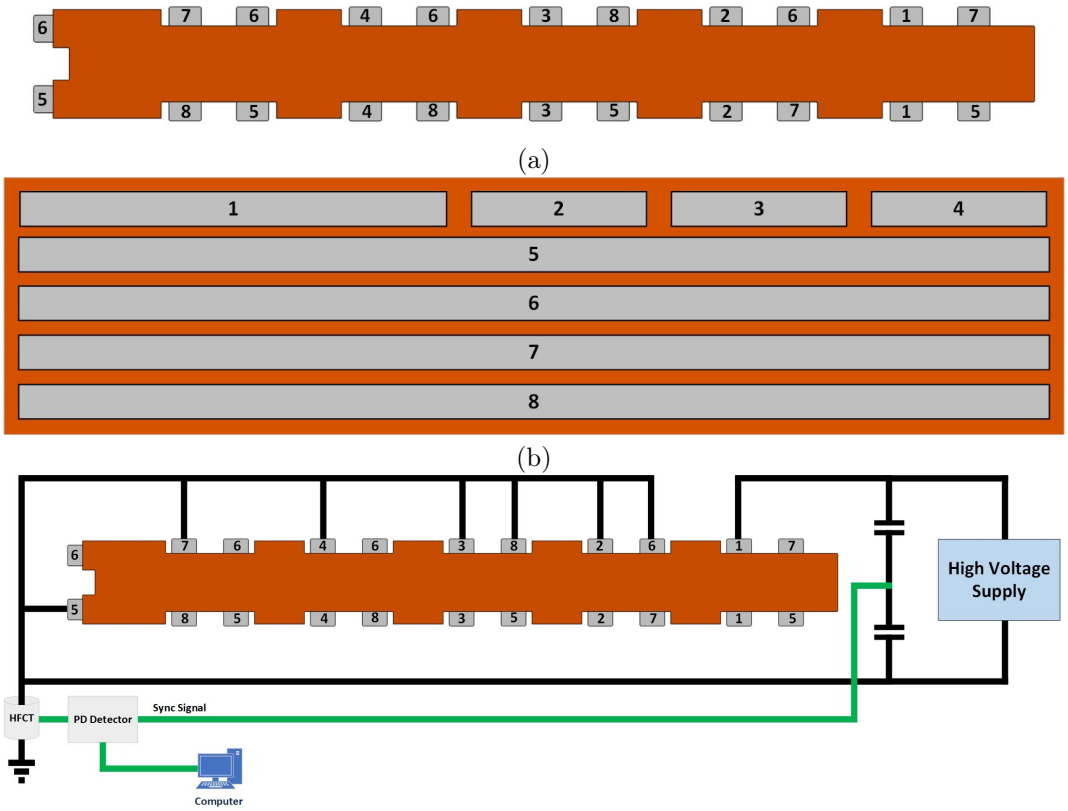

Figure 3.2: (a) Top view of the laminated busbar with eight conductive layers. Terminals with the same number are interconnected. (b) Side cut through the laminated busbar showing the arrangement of the layers. (c) Connection and testing layout of LBB

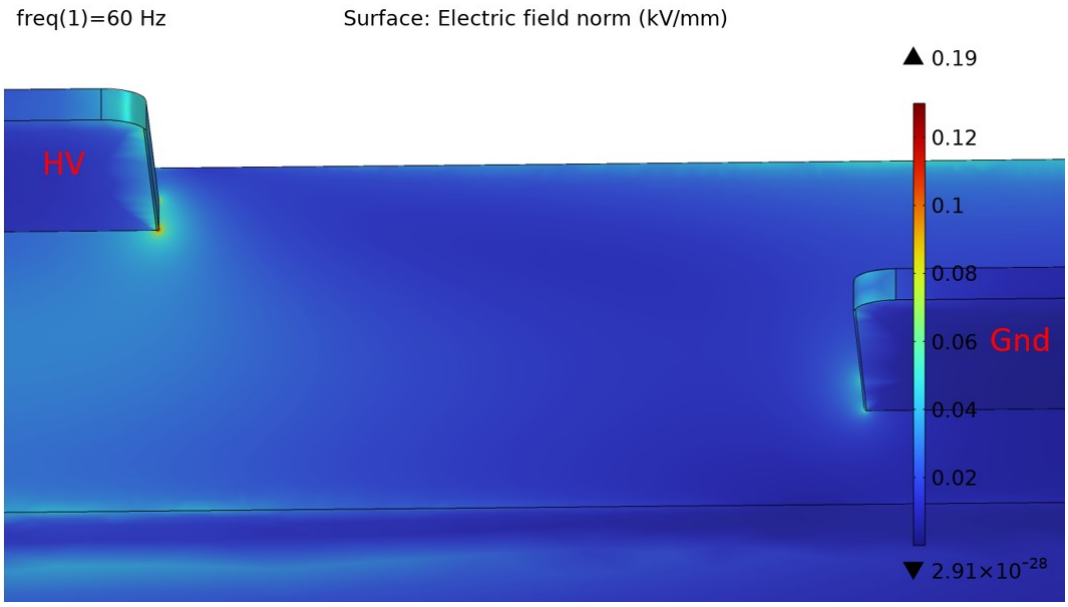

Figure 3.3: Electric Field Norm at 1kV

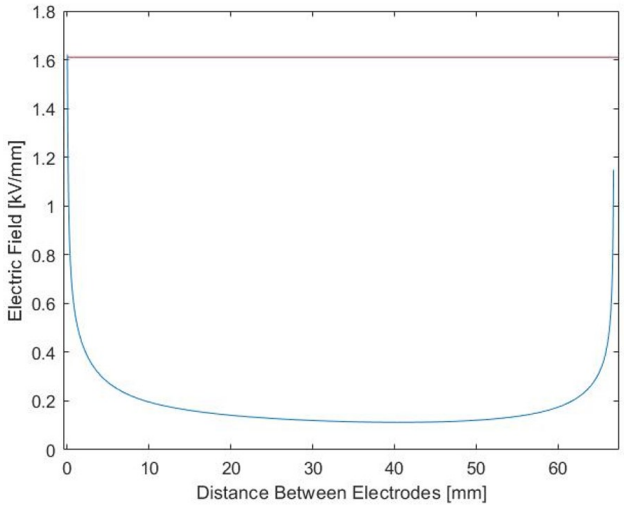

(a)

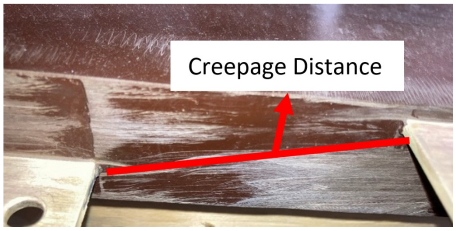

(b)

Figure 3.4: (a) Tangential electric field profile vs. distance between high voltage and ground electrode and PD inception field at 11.2kV, i.e. PDIV. (b) Shortest path between LBB terminals (creepage).

$$E_{inc} = \left(\frac{E}{p}\right)_{cr} p \left(\frac{b}{(pk_s l)^{\frac{1}{\beta}}}\right) \tag{3.1}$$

The coefficients $\left(\frac{E}{p}\right)_{cr} p$ is 8, b is 4.6, β is 2, p is the pressure, and in this case atmospheric pressure, l is the creepage distance. Due to the monotonic nature of the electric field the definition of k_s is

$$k_s = \frac{l(0.95E_{max}^{Tan}) - l(0.8E_{max}^{Tan})}{l} \tag{3.2}$$

Variable Emax is the maximum value on the field profile, and d is the distance between electrodes. Accordingly, l(0.95Emax) is the length (distance from electrode border) corresponding to 0.95 times the maximum field, as derived by the simulation of the field profile. The surface discharge inception voltage is defined as the voltage at which the tangential component of the electric field exceeds the inception field threshold. The results of the simulations combined with the theoretical model provide theoretical inception values for each terminal in Table 3.1. The graphical interpretation of the inception field can be seen for terminal one, with inception defined as the voltage which the electric field exceeds the threshold field shown in Figure 3.4. The electric field profile for each of the terminals are highly similar, with minor variations in the maximum value but with the same basic shape.

Table 3.1: AC Laminated Bus Bar Theoretical Inception Field For Each Terminal

High Voltage Terminals	Theoretical Inception Field [kV/mm]	Theoretical Inception Voltage [kV]	Distance Between Terminals [mm]	Measured Average Roughness [μm]
Terminal 1	1.61	11.2	66.8	2.1
Terminal 2	1.52	10.6	66.6	2.7
Terminal 3	1.54	10.8	66.7	1.8
Terminal 4	1.58	11.0	66.8	1.3

3.2.1 Simulation Meshing

The meshing of the laminated bus bar triple point is shown in Figure 3.5 with significant refinement in the area of the triple point with coarsening allowed further from the triple point. The area where the mesh is coarsened the electric field is of little interest regarding the phenomena of surface discharge. Also the electric field itself is small and uniform (with only small spatial variation) so refinement is not necessary.

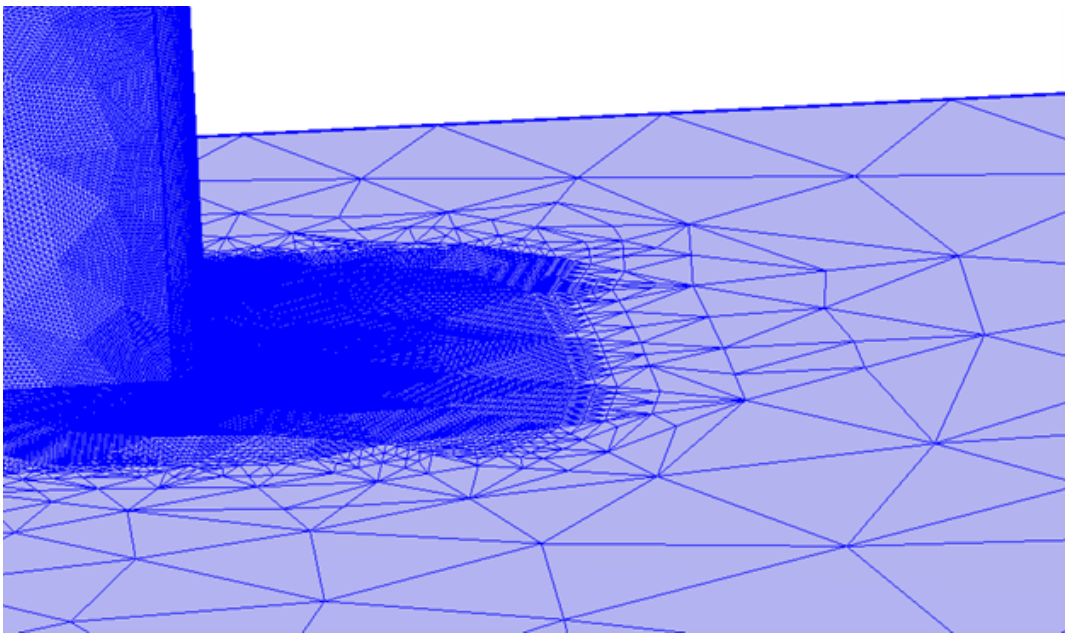

Figure 3.5: Laminated Bus Bar Meshing

3.2.2 Testing Procedure and Results

The test procedure chosen to acquire PDIV estimations for each of the terminals (starting with terminal 1) is as follows:

1. The test set up is in Figure 3.2(c) with terminal 1 connected to high voltage, and each of the other terminals grounded.
2. The voltage was increased at a constant rate of (2kV/minute) until partial discharge was incepted.
3. The partial discharge inception voltage was recorded, as well as the phase resolved partial discharge pattern at 1.2x PDIV.
4. The test was repeated 3x, with high voltage applied terminal (terminals 1, 2, 3 and 4) independently and subsequently.
5. The surface roughness at each LBB Terminal was measured.

The statistical framework used for the measurement of the PDIV is the Weibull distribution which is defined as:

$$F(s) = 1 - e^{-(\frac{s}{\alpha})^{\beta}} \tag{3.3}$$

In this case s is the measured PDIV values and α and β (the scale and shape parameter) are found through a maximum likelihood estimation algorithm.

The results from the theoretical model for the inception fields and inception voltages compared to those measured are summarized in Table 3.2 and the Weibull Probability plots shown in Figure 3.6. The measured partial discharge inception voltages align closely with those predicted using the model with the maximum error less than 5%. In addition the models do not account for the surface roughness which is likely the source for the error. The Weibull plots are used as in repeated measurements statistical uncertainty is guaranteed due to the stochastic nature of partial discharge measurements, and this statistical variation should be captured. Each of the terminals also exhibit a similar partial discharge inception voltage, which makes sense due to the similarity in the triple point. The difference in the triple point is due to the different angle of minimum distance between the terminals.

Table 3.2: AC Laminated Bus Bar Measured Inception Voltages

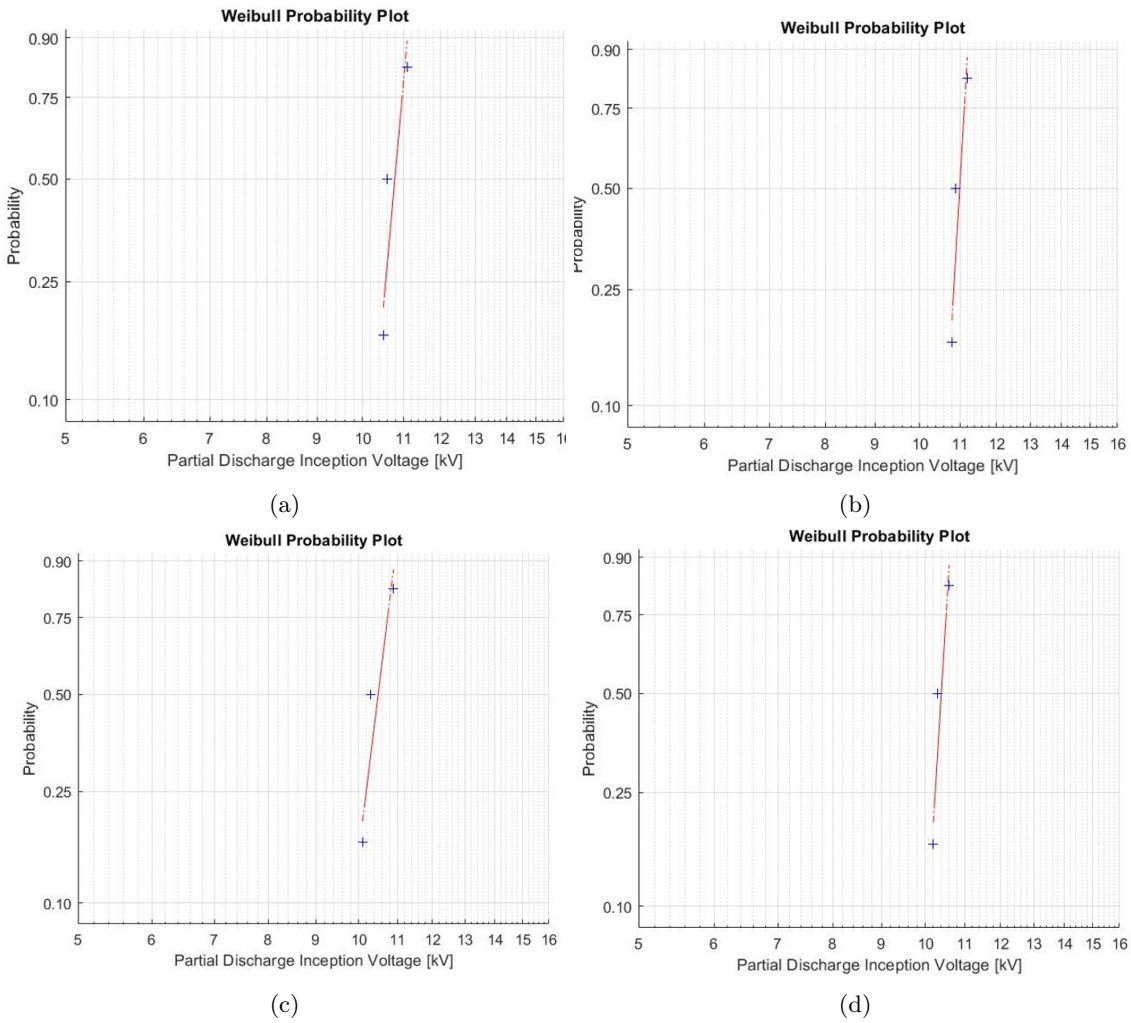

Figure 3.6: Weibull Plots of measured surface discharge inception voltage values: (a) Terminal 1 with α = 10.9kV and β = 41.6 and (b) Terminal 2 with α = 11.1kV and β = 66.5 (c) Terminal 4 with α = 10.6kV and β = 31.8 and (d) Terminal 3 with α = 10.5kV and β = 62.9

High Voltage Terminals	Theoretical Inception Voltage [kV]	Measured Inception Voltage [kV]	Distance Between Terminals [mm]	Error from Theoretical to Measured [%]
Terminal 1	11.2	10.9	66.8	2.6%
Terminal 2	10.6	11.1	66.6	4.5%
Terminal 3	10.8	10.6	66.7	1.8%
Terminal 4	11.0	10.5	66.8	4.5%

One key tool in understanding the discharge typology is the innovative software implemented by Montanari et. al. which is able to automatically Separate recorded signals, Recognize noise and PD pulses, and Identify (for the latter) of the type of PD (internal, surface or corona). An example of this at 1.1x partial discharge inception voltage for the LBB is displayed in Figure 3.7. It collects the global PRPD pattern ((a)), an

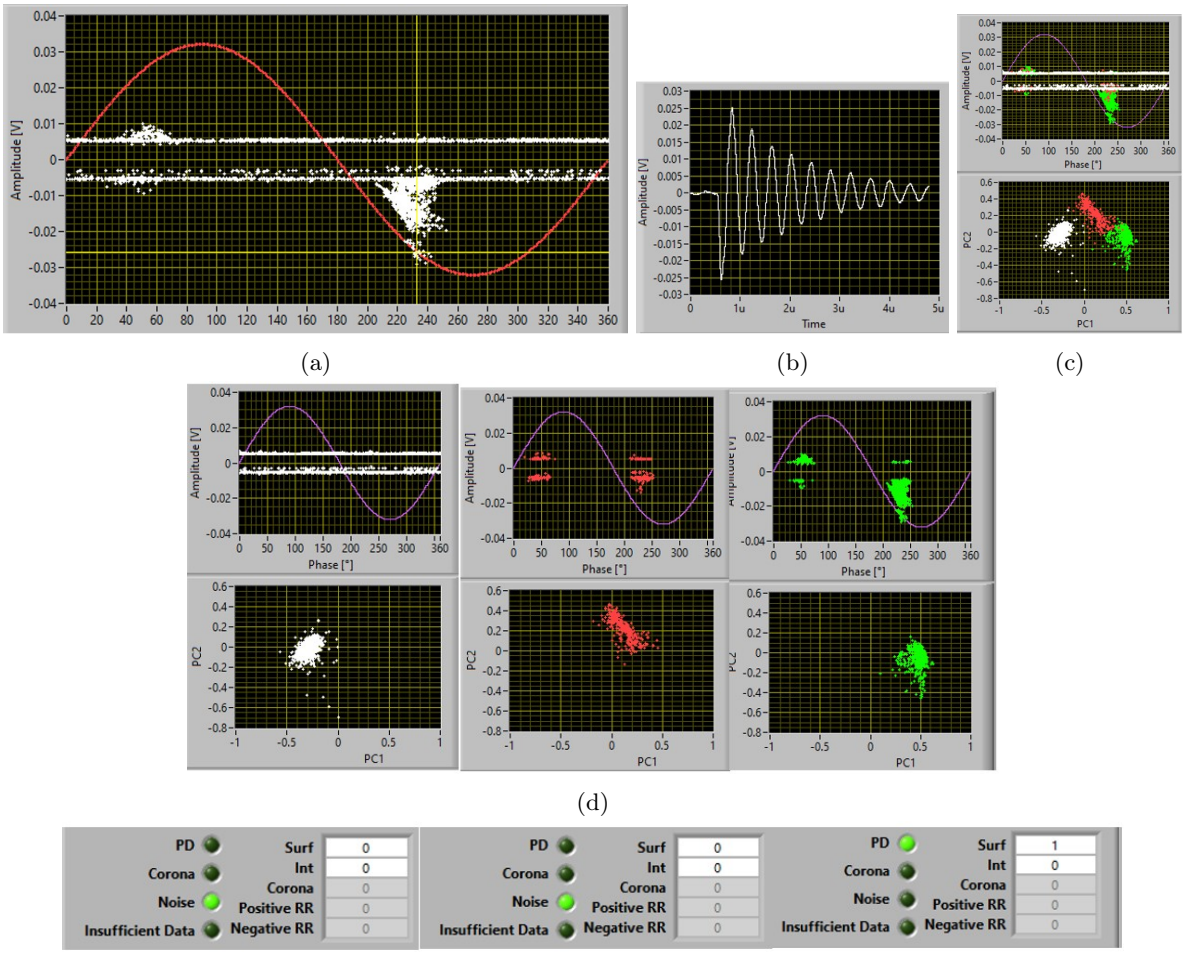

Figure 3.7: (a) Global PD pattern 12.1kV, (b); PD pulse, (c); PCA map with clustering (d); PD sub patterns (e) and Identification of 100% surface

example of a PD pulse, the separation map with sub-patterns ((c), (d)), and automatic identification of the type of source generating PD ((e)).

As can be seen, identification addresses PD entirely to surface discharges (likelihood 100%) as expected with the theoretical model and simulation which provides insight into the laminated bus bar design. A critical observation can be made by simulation of the electric field at the triple point at 3x the original creepage distance (66mm to 200mm) shown in Figure 3.8. Mainly the decrease in electric field is not proportional to the increase in creepage distance. When the surface discharge model is applied the theoretical inception voltage only increases from 10.6kV to 12.7kV. Thus if the design voltage was 13kV the only feasible way to increase the partial discharge inception voltage would be to change the terminal (and triple point) geometry [25].

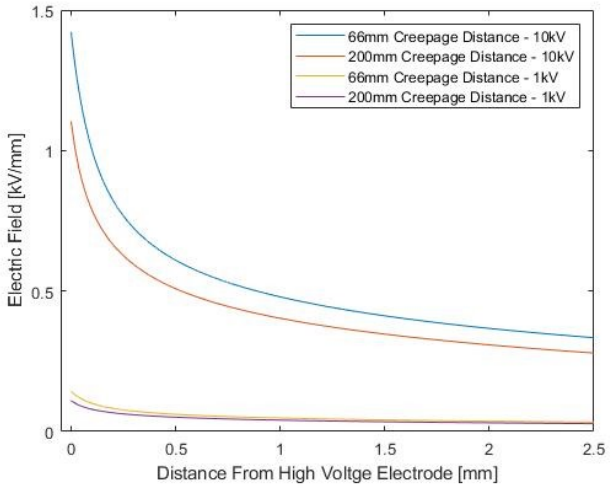

Figure 3.8: Maximum tangential electrical field as a function of distance from HV electrode, for 66mm (nominal creepage distance of the LBB Terminals) and 200mm at both 1kV and 10kV.

3.3 Impact of Surface Roughness on Discharge Inception

A second factor which can influence the partial discharge inception voltage is the rough surface which is found at the terminal triple point. During the manufacturing process the laminated bus bar was sanded at the terminals to increase the roughness shown by Figure 3.10 which motivates a further investigation into the influence on surface discharge inception of the roughness. To find the impact of the surface roughness a second test configuration using two electrodes on four levels of erosion (no erosion, mild erosion, high erosion and non-local erosion). The test set up is shown in Figure 3.11 and the simulated electric field profiles are shown in Figure 3.12. The simulated electric field profiles allows for a theoretical inception voltage to be calculated assuming an eroded surface and the reference inception voltage in Table 3.3

Table 3.3: Surface Roughness Theoretical PDIV Table

Electrode Distance	E_{inc} [kV/mm]	Theoretical PDIV [kV]
10mm	1.17	11.5
15mm	1.18	13.4

The surface partial discharge inception voltage was measured by the test arrangement of Figure 3.9, using flat Kapton specimens. Four test samples with varying levels of roughness (uneroded, mild erosion, high erosion, and non-local erosion) were considered. The fourth case (non-local erosion) has increased roughness in between the electrodes, and not at the triple points, as shown in 3.10. The voltage was slowly increased at a rate of about 2kV/min and the test at each voltage was repeated 3x.

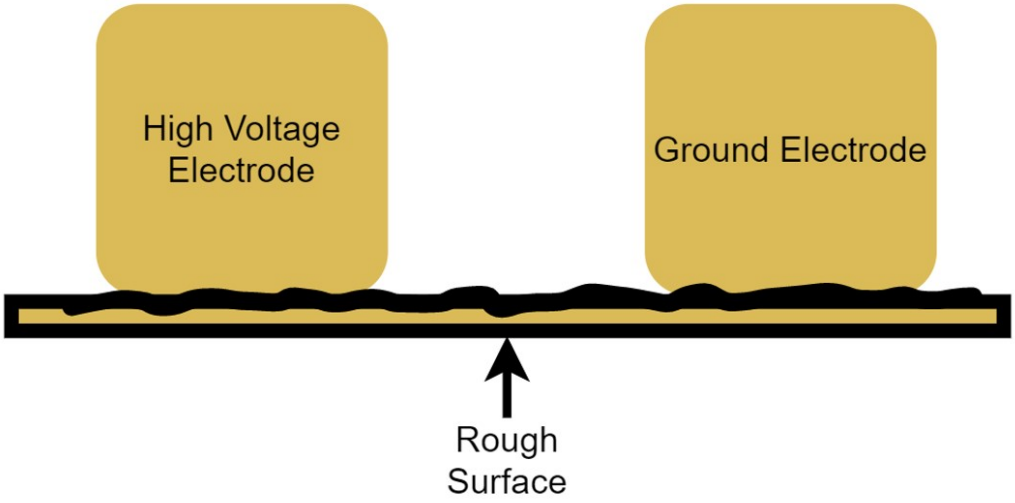

Figure 3.9: Test Set Up to Quantify the Impact of Surface Roughness

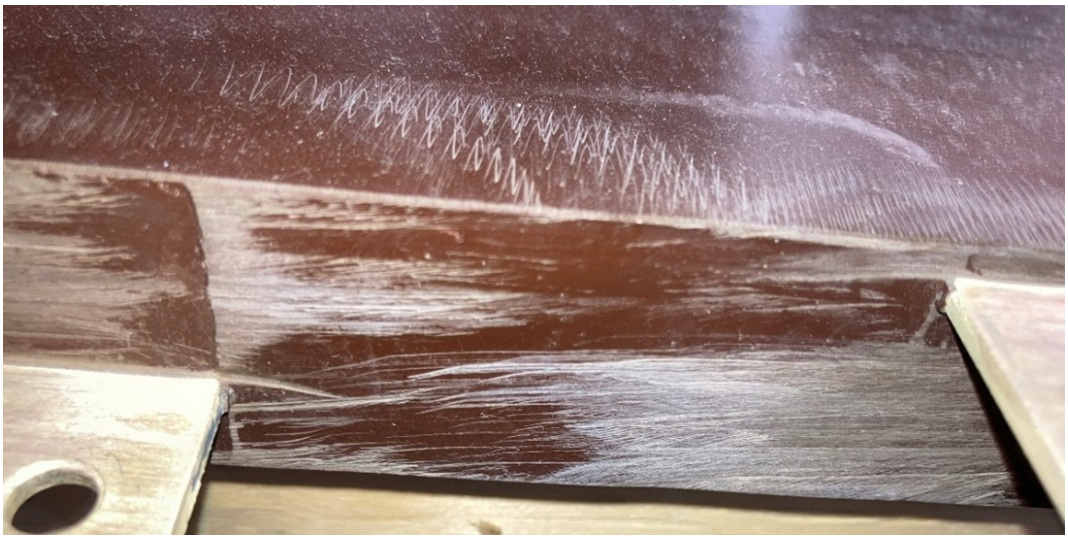

Figure 3.10: Surface Roughness of the Laminated Bus Bar

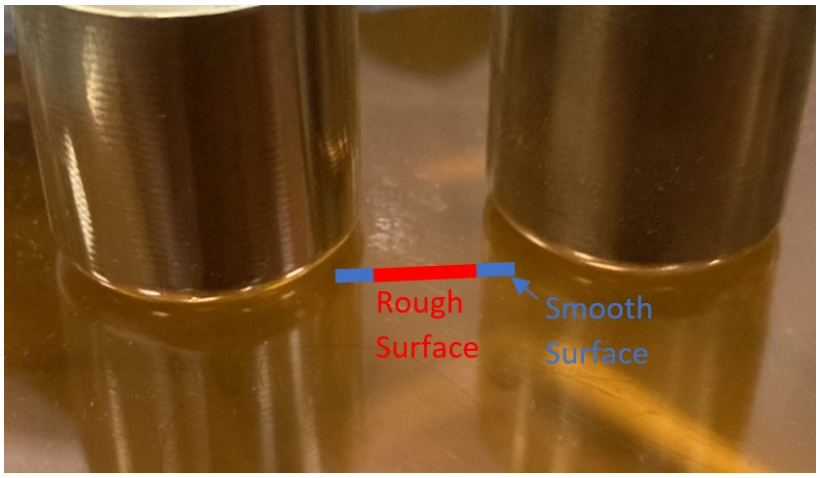

Figure 3.11: Picture of Surface Roughness Test Configuration

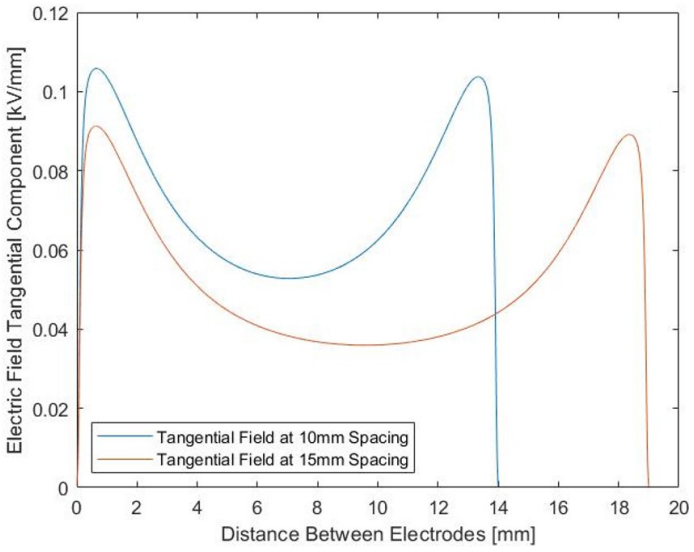

Figure 3.12: Tangential Field of Electrodes at 1kV

The result of these tests are shown in Table 3.4 and it is seen that the roughness slightly increases the PDIV if it is local to the triple point. In the laminated bus bar the surface roughness was created as a result of sanding as is the case with Kapton. The material is different but they have very similar relative permittivity ($\epsilon_r = 4$ for EPR vs. $\epsilon_r = 3.5$ for Kapton). There is also a difference in the electric field profile as well, but the discharge phenomena is the same and the qualitative impact of roughness is comparable. If the roughness is not local to the triple point has no impact on the PDIV. The impact of non local is consistent considering the initial discharge initiation occurs near the point of maximum tangential electric field.

Table 3.4: Surface Roughness Measured PDIV Table

Roughness	Arithmetic Mean Roughness [μm]	PDIV at 15mm [kV]	PDIV at 15mm [kV]
No Erosion	0.07	12.3	14.1
Mild Erosion	0.14	12.7	14.5
High Erosion	1.15	13.3	15.1
Non-Local Erosion	0.75	12.3	14.1

3.4 Discussion of AC Results

Due to the typical application of laminated bus bar application in power electronic based systems the voltage stress applied is modulated. As a result of the modulated waveform the electric field is driven by the relative permittivity, and depending on the application can either be completed AC or have a DC offset. In the case where the applied voltage is AC or modulated AC, these results provide a characterization of the bus bar.

Furthermore per IEC 61800-5 a 63mm creepage distance should correspond to a 16kV voltage rating which is 20% greater than the measured partial discharge inception voltage. Even if the creepage distance is greater than the measured PDIV, or if the creepage distance is tripled corresponding to a $>$ 32kV voltage rating the new PDIV would only be 14.7kV. This result shows that creepage does not provide insight into surface discharge inception under non-uniform electric fields. Creepage is an essential concept as it relates to the phenomena of flashover, which is a discharge event that fully crosses the insulator surface between terminals. Additional consideration regarding triple point design is necessary to prevent partial discharge which can drive aging and would reduce the life of the bus bar. The analytic and simulation based approach can be used during design to prevent the discovery of partial discharge at the testing stage resulting in a standard violation.

3.5 Laminated Bus Bar under DC Operation

The laminated bus bar can also have a DC mode of operation in which case the electric field is driven not by the permittivity but also the conductivity. This adds a complication to the computation of the electric field as the conductivity has a non-linear dependence with respect to the electric field and temperature:

$$\sigma(T, E) = \sigma_0 e^{\alpha(T-T_0)} e^{\beta(E-E_0)} \tag{3.4}$$

Where σ_0 is the reference conductivity, at a reference temperature (T_0) and electric field (E_0). The temperature dependence is modeled by α and the electric field dependence is modeled by β. A second complication is that the conductivity (bulk) and conductance (surface) while modeled by the same equation in general have different parameter values. Both have functional dependence on electric field E and temperature T The parameter values are found by conductivity testing with the cells shown in Figure 3.13.
Conductivity is tested by applying a DC voltage to a sample which has been sputtered (thin layer of gold has been deposited on the surface of the sample to ensure a good electrical connection). The conductivity is then measured in time, untill a steady state conductivity is reached. When the voltage is first applied the electric field will be primarily capacitve, and it will decay in time to a steady state DC current through the insulator. The relationship between the electric field applied and the conductivity is not linear, so the test must be applied at multiple different values of electric field to fit the parameter β. The same test is then repeated at 3 different temperatures to fit the parameter α.

Table 3.5: Conductivity and Conductance Measurements

	$\sigma_0[Siemens]$	$\alpha\ [C^{-1}]$	$\beta[mm/kV]$
Bulk σ	4.4×10^{-16}	0.07	0.13
Surface σ	2.8×10^{-14}	0.06	1.335

The conductivity measurements allow for the electric field to be simulated, with the electric field norm shown in Figure 3.14. The electric field simulation allows for the theoretical inception voltage to be calculated based on equations on 3.1 and 3.2.

The voltage at which the electric field profile intersects with the inception field is the partial discharge inception voltage. As in the case of AC, the maximum electric field is along the minimum distance between the terminals or the creepage distance shown by figure3.15

A factor which is different from AC is the temperature dependence of the conductivity which will intern change the electric field. Both the absolute temperature and temperature gradients can change the electric field and the resultant partial discharge inception voltage. In the case for the laminated bus bar assuming

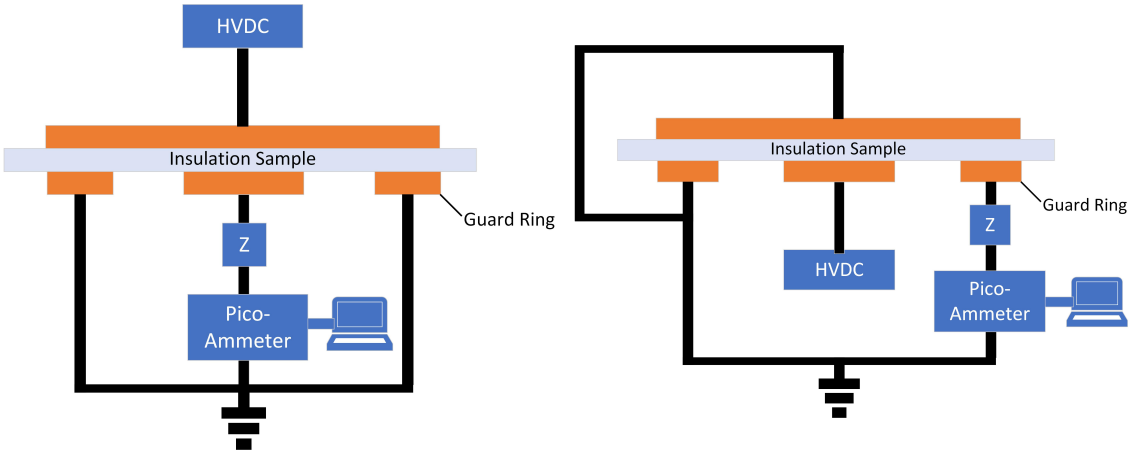

(a) (b)

Figure 3.13: (a) Bulk Conductivity Test Set Up (b) Surface Conductance Test Set up

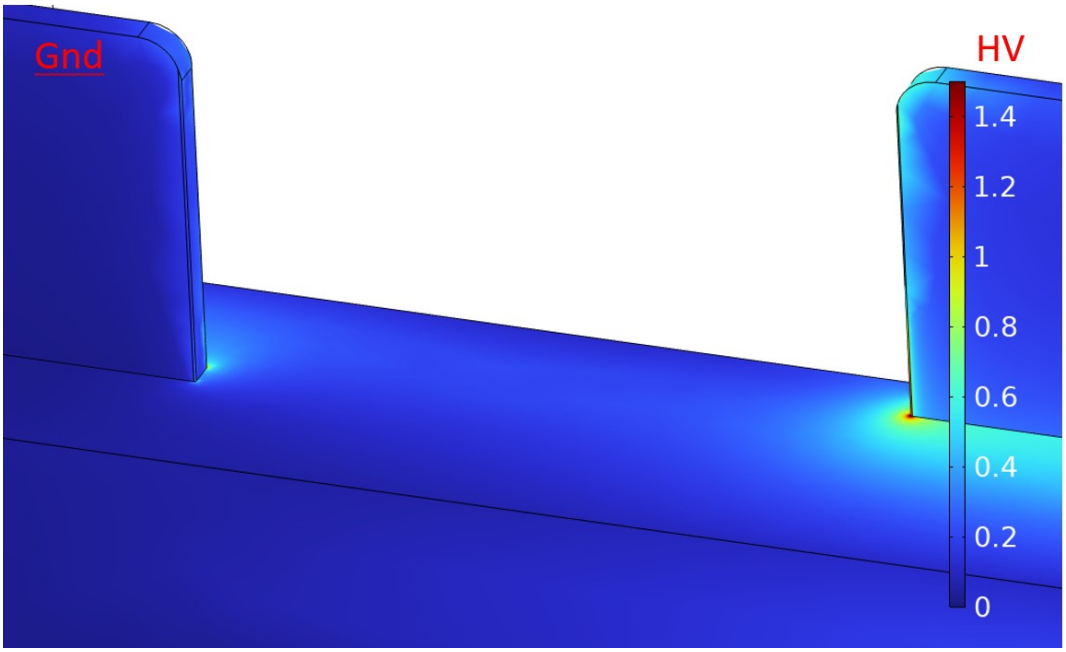

Figure 3.14: Electric Field Norm DC at 15kV

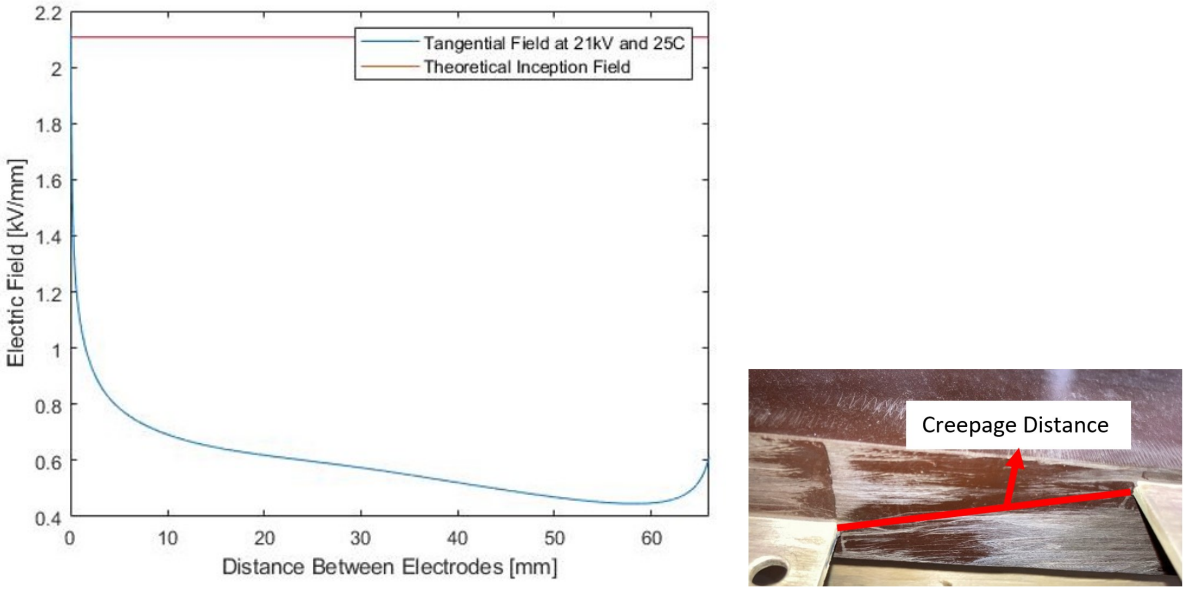

(a) (b)

Figure 3.15: Tangential electric field profile vs. distance between high voltage and ground electrode and PD inception field at 21.5kV, i.e. PDIV. (b) Shortest path between LBB terminals (creepage).

a uniform temperature of 25C (room Temperature) and 60C the change in partial discharge is small shown by Figure 3.16. One factor not considered here is the dependence of gas parameters on temperatures. The conduction mechanisms which can drive the availability of electrons and presence of space charge have a dependence on temperature themselves. Thus an increase in temperature may result in a small change in the gas parameters used to model the surface discharge inception voltage. A final consideration of DC is the impact of transients. Under transient conditions the electric field will initially be driven by the relative permittivity and will then evolve to being driven by the conductivity. A DC system will always have the possibility of a transient as a result of a fault or load step. It is also may not be possible to control transients to ensure that the rate of change is small (such that the electric field does not become capacitive). The second impact is that the surface discharge inception during these transients is significantly lower than during steady state, thus partial discharge could occur during DC transient conditions) [31].

3.5.1 Test Procedure and Results

The PD test procedure under DC conditions is as follows:

1. The test set up is shown in 3.2, with terminal 1 connected to high voltage, and each of the other terminals grounded with the test conducted at room temperature of 25C.

2. The voltage is increased at a constant rate of (0.1kV/s) till 12kV, then it is raised in 0.5 kV steps, each

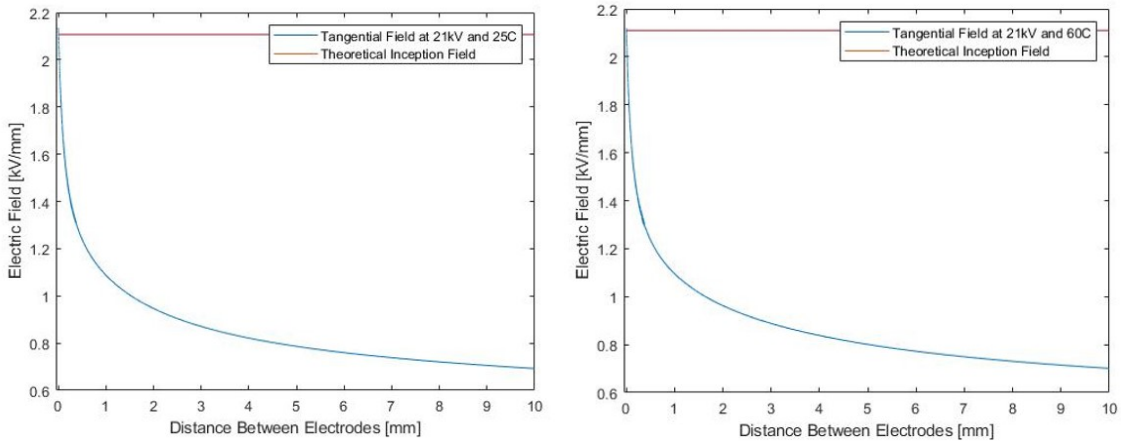

(a) (b)

Figure 3.16: Temperature Dependence of the Electric Field at (a) 25C (b) and 60C

step lasting 5 min. Above 12 kV and at each voltage step, 5-minute PD acquisitions are taken up to 1.2xPDIV.

3. The partial discharge inception voltage is recorded, and the partial discharge pattern at 1.2x PDIV.

4. The test is repeated 3 times on each terminals (terminals 1, 2 and 3), with recovery time between one test and the other of at least 1 h.

5. A transient analysis is carried out on each of the terminals. Where the voltage is increased from 0kV to 0.9x DC PDIV in 1 second, in order to estimate the transient PDIV, which is expected to be very close to the PDIVAC presented in the previous report

6. Steps 1-4 are repeated at 60C. The measured values of PDIV are reported and compared to the theoretical model for the inception field and voltage from model in Table 3.6. The error between the theoretical model at 25C very small (less than 5%), and the change between the theoretical PDIV from 25C to 60C is insignificant. The observed slight decrease in PDIV is likely due to the slight temperature dependence of the gas ionization coefficients.

Table 3.6: Surface Roughness PDIV Table

High Voltage Terminals	Theoretical Inception Voltage	Measured Inception Voltage at 25C [kV]	Measured Inception Voltage at 60C [kV]	Error from Theoretical to Measured at 25C.
Terminal 1	21.0	22.0	20.5	4.5%
Terminal 2	21.0	22.0	20.5	4.5%
Terminal 3	20.5	21.5	20.0	4.7%
Terminal 4	21.0	22.0	20.5	4.5%

The measured time resolved partial discharge pattern is shown in Figure 3.17, several observations can be made from this partial discharge pattern. The first PD pulse did not occur until 50s after the voltage ramp started, (and the voltage ramp was very slow) so it can be easily established this is steady state PD. The repetition rate of the PD was low with approximately 1 partial discharge event per minute. Contrasted with AC partial discharge, if incepted can result in hundreds or thousands of pulses each second. This puts a weight on the aging potential, the risk of premature aging and failure if partial discharge incepts under AC is much greater compared to DC. Even in the case where a fast transient was applied to the LBB quickly changing the voltage from 0kV to 15kV DC as in Figure 3.18, more pulses occurred as a result of the 1 second transient than under 5 minutes of steady state PD at 1.2x PDIV. The primary risks of DC insulation systems with respect to partial discharge are as follows.

1. Space charge
2. DC ripple which is of sufficient magnitude to incept partial discharge
3. Frequent transients

The first risk of space charge is unique to DC as the electric field does not change polarity in time, free charges can move into the bulk or along the surface of an insulator which decreases the global electric field (as a result of the previously mentioned conduction mechanisms). This may sound advantageous, but it can result in a large local field enhancement in unintended locations resulting in partial discharge, or in the worst case even insulation failure. Coupled to that fact, if significant space charge accumulates and a polarity reversing transient occurs (single line to ground fault in an ungrounded power system), the transient electric field can be significantly amplified. An additional risk arises if DC ripple is present. In this case the electric field will have a time variation with a DC offset, which means that space charge can accumulate over time and shift the electric field while maintaining a time varying nature. This means that if PD is incepted at a different location due to space charge accumulation PD could occur with a repetition rate driven by the ripple [22].

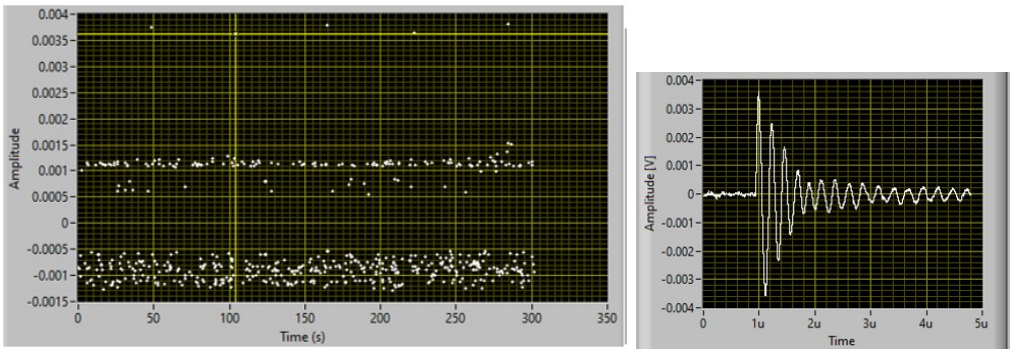

(a) (b)

Figure 3.17: (a) DC Steady State Partial discharge (b) Pulse Waveform

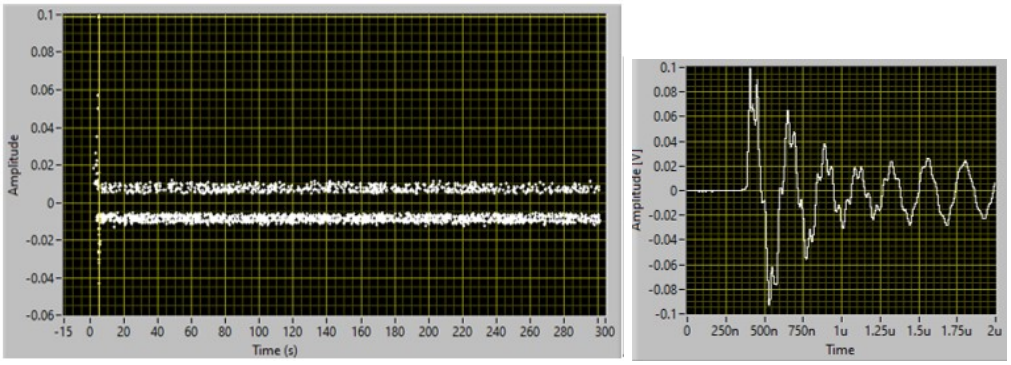

(a) (b)

Figure 3.18: Time Resolved Partial discharge pattern for DC fast transient from 0 to 15kV

3.6 Discussion of DC Results

With power electronics a truly "DC" system does not exist, but systems with a small enough ripple can be considered as DC . Characterization of the LBB under DC stress conditions is important as it is a possible stress. Even if ripple is present the electric field will have a component driven by the DC field. As in the case of AC stress the concept of creepage is isolated from surface discharge inception with an increased creepage distance. The additional challenge of space charge could also have an impact on surface discharge inception which itself warrants future study. From the measurement it is observed that the AC partial discharge inception is significantly lower than that of DC, a large reason for this is the non-linear conductivity of the epoxy polymer resin which increases the conductivity as the electric field increases. The measurements also emphasize how different insulation designs may be when going from AC to DC or vice versa. As previously discussed the two main factors which drive the electric field, and the surface discharge inception voltage, are the geometry and type of voltage applied. For the laminated bus bar the electric field is highly non-uniform under both AC and DC applied stresses but due to the changes in the electric field profile the partial discharge inception is 11kV for AC and 21kV for DC.

The surface discharge model explored in this section through the theory, simulation and testing provides foundational physics for insulation coordination. With the ultimate goal and motivation of physics based insulation coordination for the virtual prototyping process this section constitutes a step forward to this goal.

Chapter 4

Material Characterization and Surface Erosion Testing

The first criteria for insulation system design is to be partial discharge free, this was the topic of exploration of the second chapter. A second criteria for an insulation design could be the use of partial discharge resistant materials. In order to maximize insulation life even if partial discharge is incepted. This additional criterion provides a design redundancy allowing for materials to endure even the most severe environment's. In order to characterize these materials a rapid surface erosion test is employed. This chapter will focus on the characterization of two commercially available materials, Kapton (Kapton NCR), and Corona Resistant Kapton (Kapton CR). Traditionally, life testing is completed at constant voltages till failure at an estimated probability with the data then fitted to a life model. These tests can take significant time (months or years) if fields near the design values are selected. As a result of this typical stress values occur at voltages significantly greater than the design stress. The life model for this case is defined as [22]:

$$L = \frac{f_0}{f} L_H \left(\frac{E}{E_H} \right)^{-n} \tag{4.1}$$

Where f is the frequency f_0 is the reference frequency (60hz) L_h is the reference life at reference electric field E_h and n is the voltage endurance coefficient. An example of the life lines for Kapton CR and NCR are shown in Figure 4.1 The corona resistant materials are shown to have a better resistance to partial discharge with the longer life even at higher levels of electric stress[29][27]. This form of testing is a state of the art approach for insulation assessment, but other approaches are motivated due to its length. In summary, the test procedure consists of:

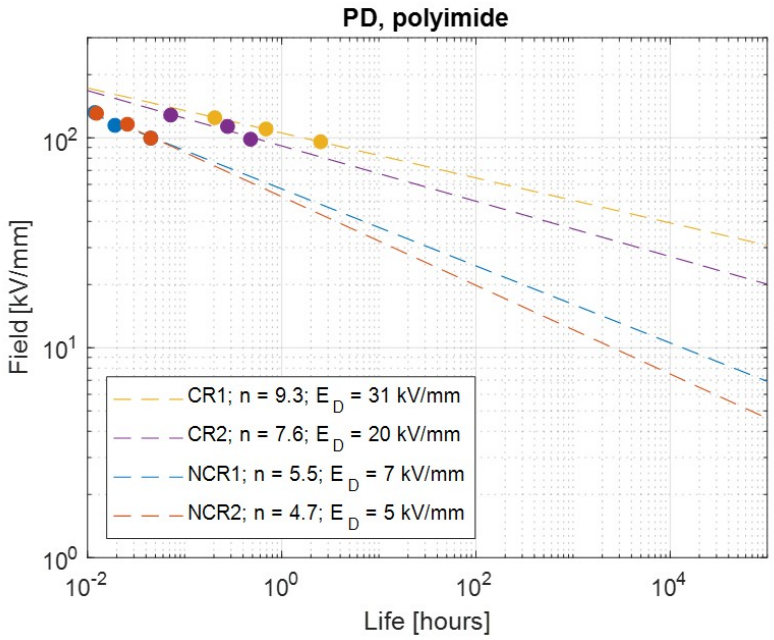

Figure 4.1: Accelerated life tests results and relevant life lines under PD for materials of the polyimide family (CR=corona resistant, NCR= non-corona resistant). 20°C, Design life, LD, = 105 h. Failure probability 63.2%.

1. Breakdown strength testing for each material with oil at the triple point (such that breakdown occurs through the material, not across the surface as creepage breakdown) using the electrode configuration shown by Figure 4.2

2. Connecting the high voltage electrode to a coupling capacitor and the AC high voltage transformer and connecting the low voltage electrode to ground. The ground passes through a high frequency current transformer, HFCT, which is the sensor for the PD measurements. Synchronization provides the phase relation between the partial discharge event and the supply voltage, which is achieved by a Rogowski coil.

3. The two test voltages are 2kV and 3kV, the power supply has built in over-current protection so it a large over-current occurred as a result of sample failure the voltage supply was protected.

4. Monitoring PD and recording the PRPD patterns, e.g., every 30 minutes.

5. Carrying out erosion assessments (by a profilometer) and microscopy observations (e.g. at 3 hours, 5 hours, 7 hours, as well as after breakdown.)

Three types of characteristics can be observed as a function of aging time for each material, 1. Optical evaluation using 600x and 2040x magnification

2, Information from partial discharge patterns and SRI (Separation, Recognition, Identification)

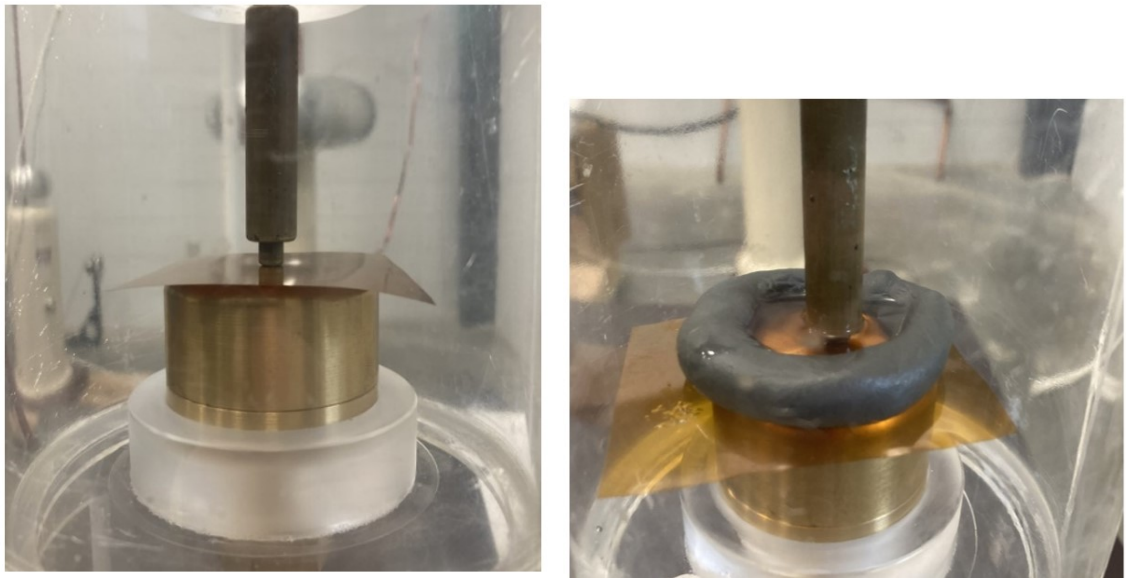

(a) (b)

Figure 4.2: Test Cell (a) Nominal Condition (b) With Oil for Breakdown Testing

3. Measurements of the average surface roughness.

Surface erosion tests can be executed much more rapidly compared to conventional life tests which is the key motivation of investigation.

4.1 Theory and Analysis

The electrode configuration and triple point are shown by Figure 4.3 and Figure 4.4 due to the curved electrodes the electric field can have both a significant normal and tangential component. As a result of both components of the electric fields tow types of discharge may occur. Gas discharge (driven by the normal E field) and surface discharge (driven by the tangential E field). Gas discharge is possible because the electrode forms an artificial cavity and the normal component of the electric field is significant.

The electric field profiles allow for calculation of both the gas and surface discharge inception voltages. These inception voltages may be calculated by [37, 36]:

$$E_{ig} = 25.2\left(1 + \frac{8.6}{\sqrt{pd}}\right) \tag{4.2}$$

$$E_{isg} = 25.2\left(1 + \frac{4.3}{\sqrt{pk_s d}}\right) \tag{4.3}$$

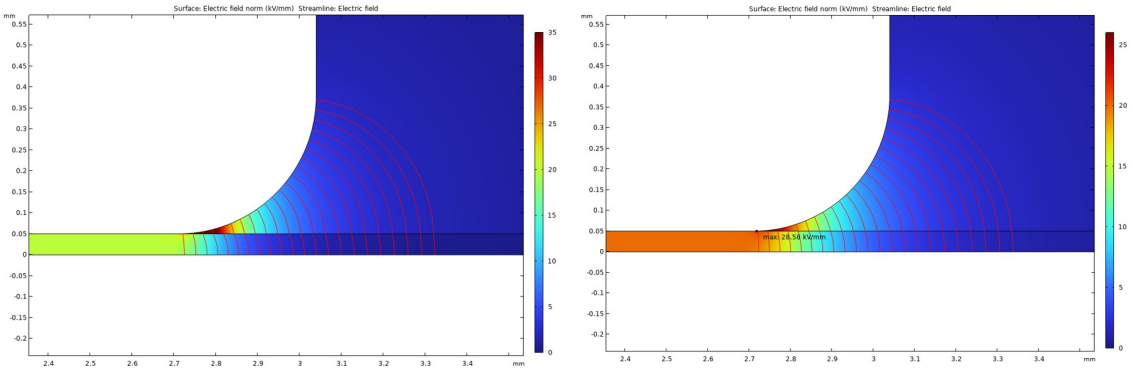

(a) (b)

Figure 4.3: Electric Field Norm in (a) air (b) and in Oil

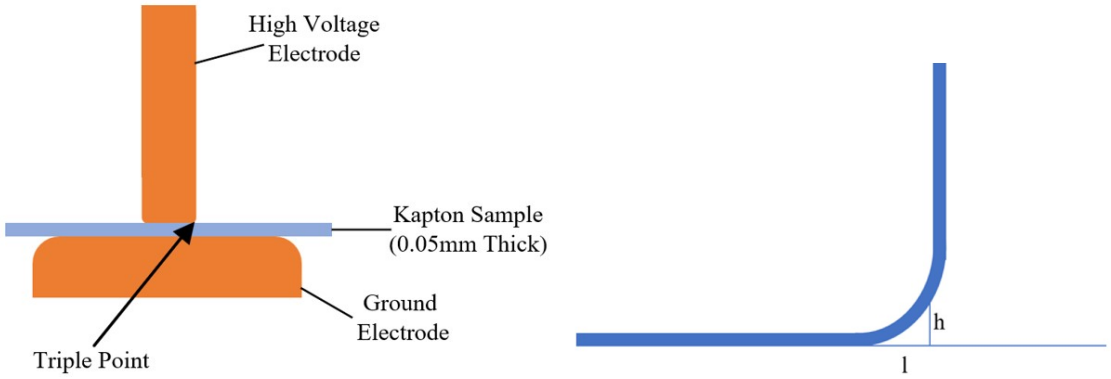

(a) (b)

Figure 4.4: Fig. 3. Electrode configuration (a) and highlight of the upper electrode contour (b)

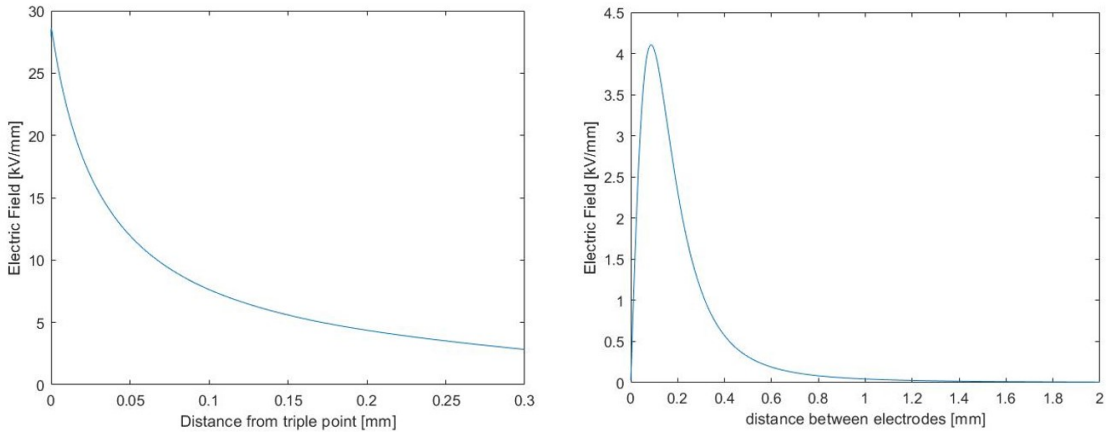

(a) (b)

Figure 4.5: Simulated electric field with electrodes as in Figs. 4.2 and 4.4 [(a) Normal field (orthogonal to specimen surface) and (b) tangential Field.] The x-axis zero is the triple point of the test cell

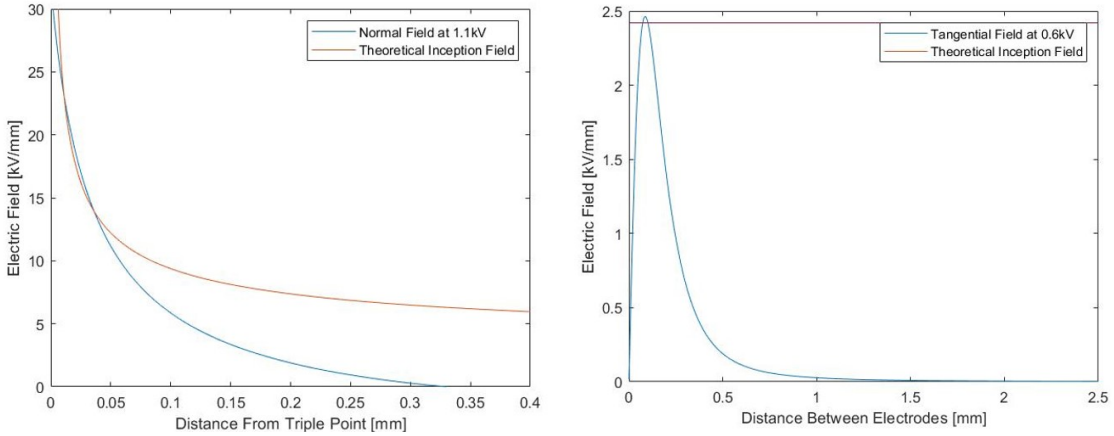

(a) (b)

Figure 4.6: Theoretical Inception Electric fields for (a) Gas Discharge at 1.1kV (b) Surface Discharge at 0.6kV

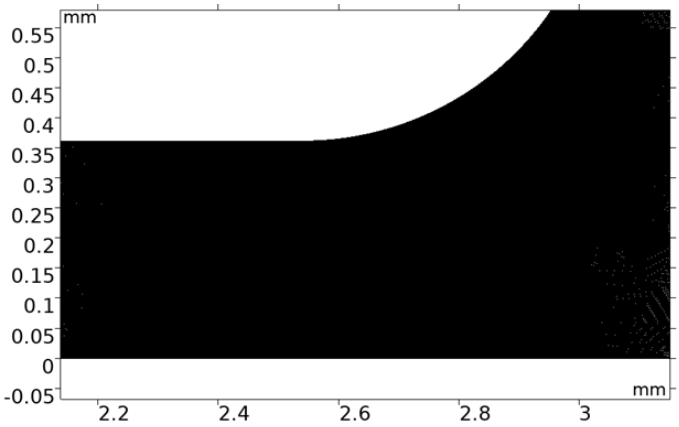

Figure 4.7: Meshing of Erosion Test Cell Triple-Point

The surface discharge inception voltage is calculated by the simulated electric field applied to the equation. Surface discharge inception theoretically occurs at 0.6kV under atmospheric pressure and gas discharge theoretically incepts at 1.1kV shown by Figure 4.6. At the test voltages of 2kV and 3kV it can be concluded that both surface discharge and gas discharge are possible. It is expected that identification of the partial discharge would be mostly surface due to the lower inception voltage.

4.1.1 Simulation Meshing

The meshing for the electric field at the triple-point is shown in Figure 4.7. Because of the cylindrical symmetry of the test cell a 2D axisymetric model can be employed which greatly increases the computational efficiency of the simulation. As a result of this the mesh can be refined even beyond what a minimum requirement for accuracy would be with minimal computational cost.

4.2 Breakdown Testing

Before conducting the erosion testing breakdown tests were completed on each of the samples to provide a threshold for breakdown testing in the event of test survival. The breakdown testing was repeated five times and fitted to the weibull distribution. It is observed that the breakdown strength for Kapton NCR is greater than that of Kapton CR. The breakdown strength was estimated in kV/mm from an electric field simulation with the triple point submerged in oil. The breakdown was observed to be at (or very near) to the triple point matching the location of maximum electric field. One factor not considered which may influence the exact breakdown strength is oil absorption into the material. This cannot be avoided however as without using oil breakdown will occur by flash-over much before breakdown through the material bulk. It is interesting to note that Kapton CR (as will be shown) is able to survive partial discharge degradation much better compared to Kapton NCR but this does not translate to breakdown strength. Breakdown strength is an important value for material selection, it should not be the only design criteria. Where α is the shape parameter corresponding the voltage magnitude and β is the scale parameter corresponding to the distribution of the measured values.

Table 4.1: Voltage for 0.05mm Kapton CRC with α = 9.5kV (approximately 237.5 kV/mm) and β = 27.7 from Weibull cdf.

Sample #	Breakdown Voltage [kV]	Estimated Breakdown Field [kV/mm]
1	10.5	263
2	9.8	245
3	10.8	270
4	10.1	255
5	10.1	252.5

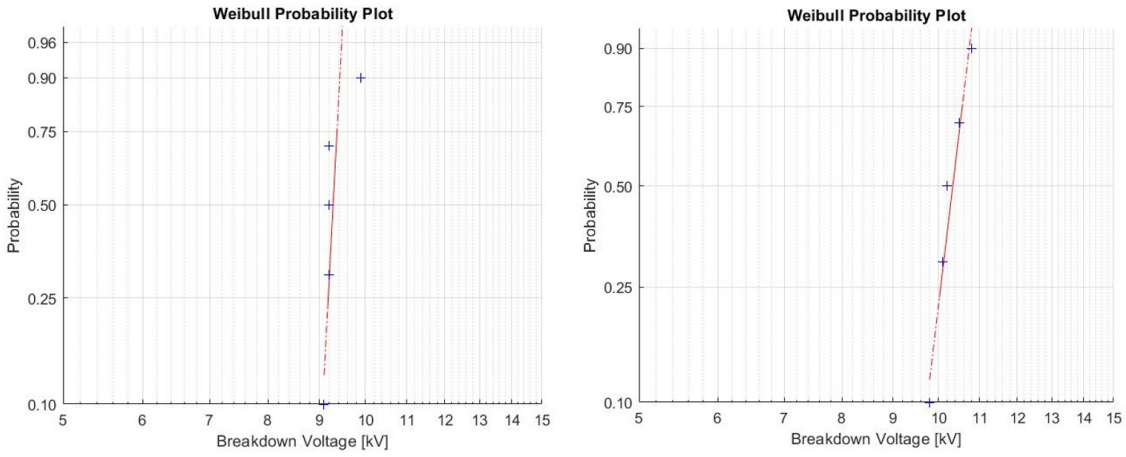

(a) (b)

Figure 4.8: Weibull plot of the 5 breakdown voltage values (a) Kapton NCR with an α =10.4 kV and β = 32.2 (b) Kapton CR with α =9.5kV and β = 27.7

Table 4.2: Breakdown Voltage for 0.05mm Kapton NCR with α =10.4 kV (approximately 260 kV/mm) and β = 32.2 from the corresponding Weibull CDF

Sample #	Breakdown Voltage [kV]	Estimated Breakdown Field [kV/mm]
1	9.9	247.5
2	9.2	230
3	9.2	230
4	9.1	227.5
5	9.2	230

4.3 Observations and Results

An observation made from the erosion testing was a result of the automatic innovative software which is able to identify the source of PD. [For both materials at the test voltages of 2kV and 3kV both surface discharge and gas discharge can theoretically incept, but surface discharge incepts at a significantly lower voltage. At the beginning of testing this theoretical premise is confirmed by the mostly surface identification of the partial discharge. It is then expected that identification of the partial discharge would be primarily surface discharge with a smaller internal component. At 2 kV the Kapton NCR materials failed at 6, 6.5 and 7 hours each respectively while for Kapton CR all three samples survived the testing (i.e. censored at 8 hours). At 3kV two of the the Kapton NCR samples failed at 4 and one failed at 4.5 hours. Two Kapton CRC

samples survived testing and one failed at 7.5 hours. While Kapton NCR has a larger breakdown strength it has a much poorer ability to endure partial discharge degradation. In addition to this observation of Kapton CR being a better choice if partial discharge could incept during the insulation systems life, several metrics can be considered. These will be discussed in sections

4.3.1 Evolution of Partial Discharge Identification

The phase resolved partial discharge pattern was recorded every 30 minutes and an interesting observation was made. As expected the identification of the partial discharge was primarily surface for both Kapton CR and NCR. After the sample began to age a transition was observed in the identification from mostly surface to mostly internal (when the sample approached breakdown). The change in the patterns for the corona resistant Kapton from 0 to 4 hours is small (there are slight differences) and the change in identification is only 9%. But the change from 4 hours to 8 hours is quite significant, which is also observed in the identification of mostly internal. For Kapton NCR the transition from 0 hours to 2 hours is small (but larger than that for Kapton CR). At 4.5 hours (just before failure) the pattern is substantially different (lower inception phase angle) and has an identification of mostly internal.

The software used has the capability for automatic acquisition and identification lays the foundation for automatic algorithms of insulation life estimation based on online measurements. This approach will be explored in detail in section 4.4, based on the observation of an identification transition as a function of surface erosion. The observed patterns, PCA Maps, and identification are shown in Figures 4.9 through Figure 4.14.

In addition to the change of the identification in time the 95% confidence interval of the amplitude and the partial discharge repetition rate shown in Figure 4.15. These measurements can also provide further insight for an algorithm to calculate the aging which has taken place.

4.3.2 Surface Roughness Measurements

In addition to the observation of the partial discharge analytics the surface roughness was periodically measured for each of the samples. Partial discharges damage the sample and will damage the material at a different rate for each material. In particular corona resistant Kapton is able to resist degradation as a result of nanofillers which significantly decreases the rate of erosion as a result of partial discharge. The erosion measured in terms of average roughness observed for Kapton NCR is twice that of Kapton CR shown by Figure 4.16.

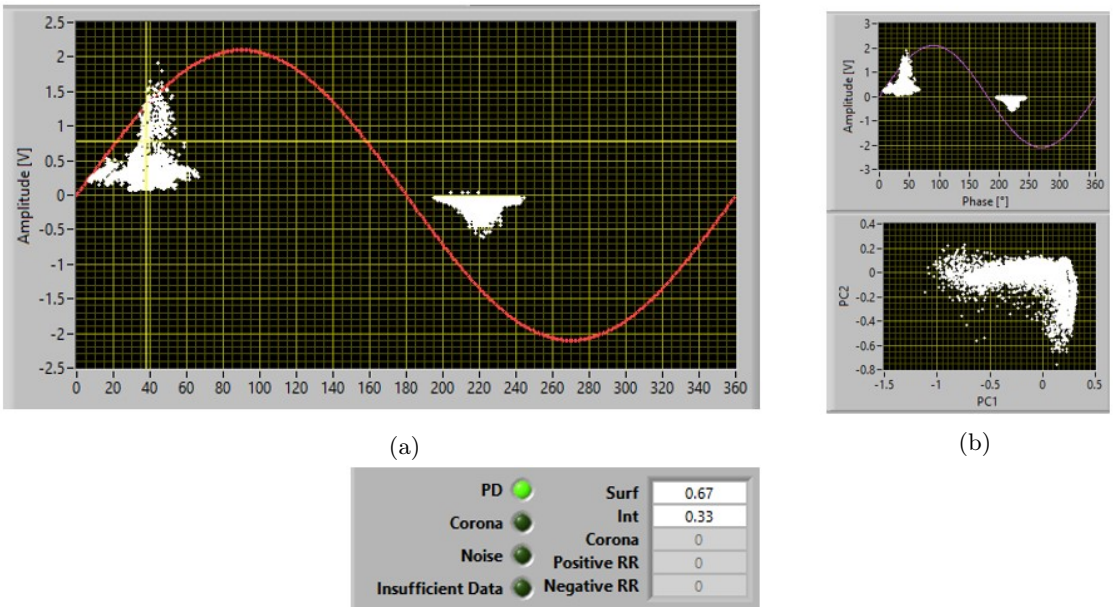

(a) (b)

(c)

Figure 4.9: (a) Kapton CRC Phase-resolved PD (PRPD) pattern (b) separation (PCA) map (c) Identification at the beginning of aging (t=0) for 2kV

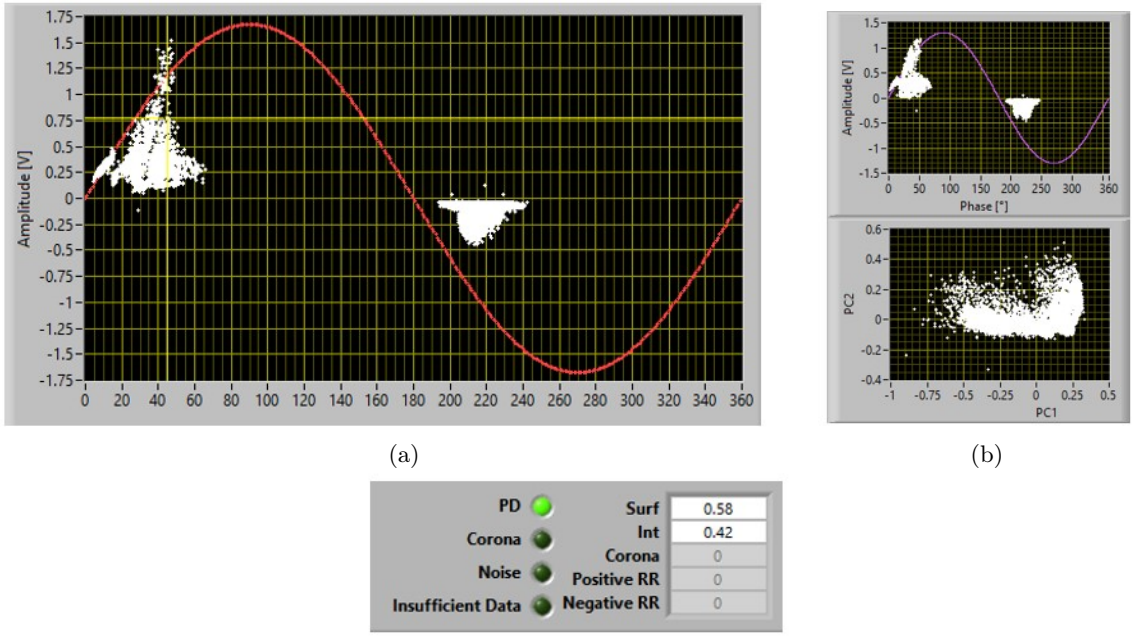

(a) (b)

(c)

Figure 4.10: (a) Kapton CRC Phase-resolved PD (PRPD) pattern (b) separation (PCA) map (c) Identification in the middle of aging (t=4) for 2kV

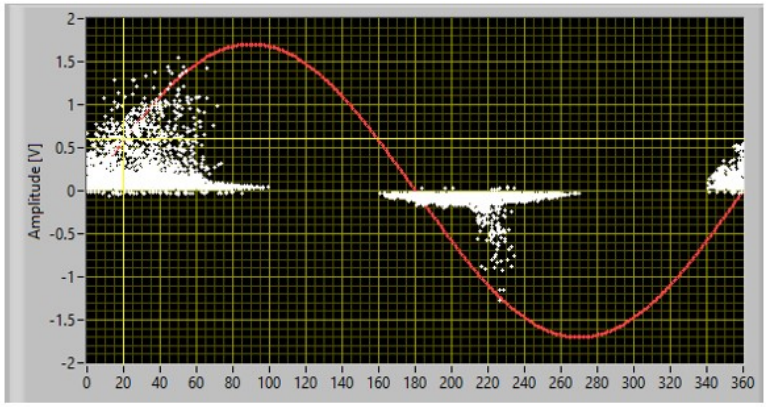

(a)

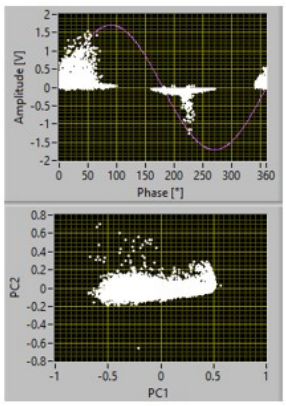

(b)

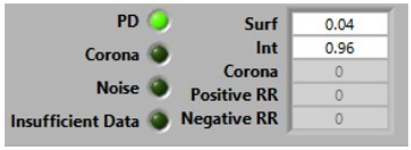

(c)

Figure 4.11: (a) Kapton CRC Phase-resolved PD (PRPD) pattern (b) separation (PCA) map (c) Identification at the end of aging (t=8) for 2kV

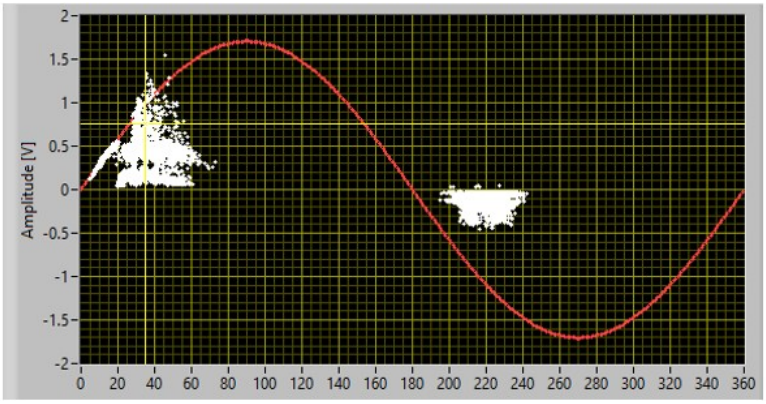

(a)

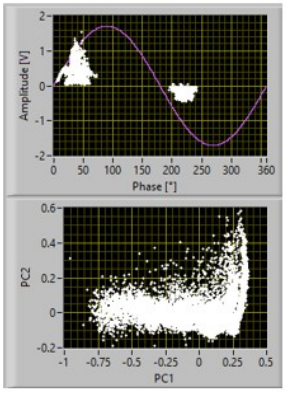

(b)

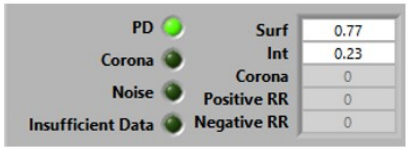

(c)

Figure 4.12: (a) Kapton NCR Phase-resolved PD (PRPD) pattern (b) separation (PCA) map (c) Identification at the beginning of aging (t=0) for 2kV

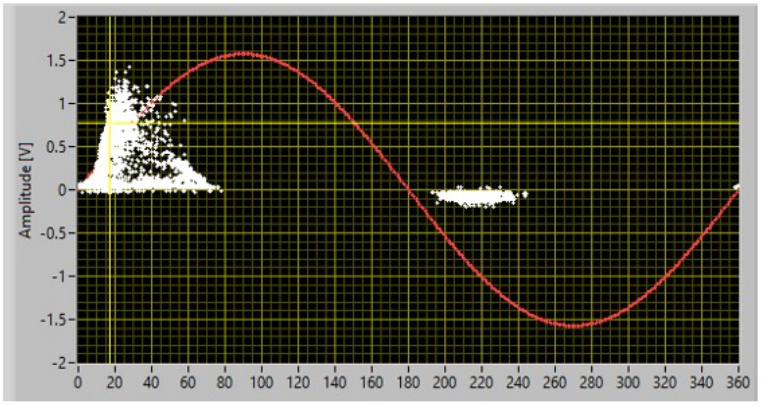

(a)

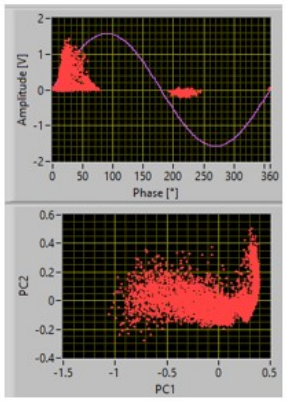

(b)

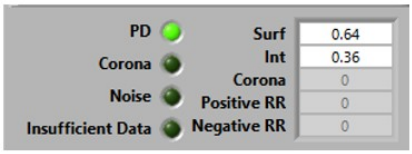

(c)

Figure 4.13: (a) Kapton NCR Phase-resolved PD (PRPD) pattern (b) separation (PCA) map (c) Identification in the middle of aging (t=2) for 2kV

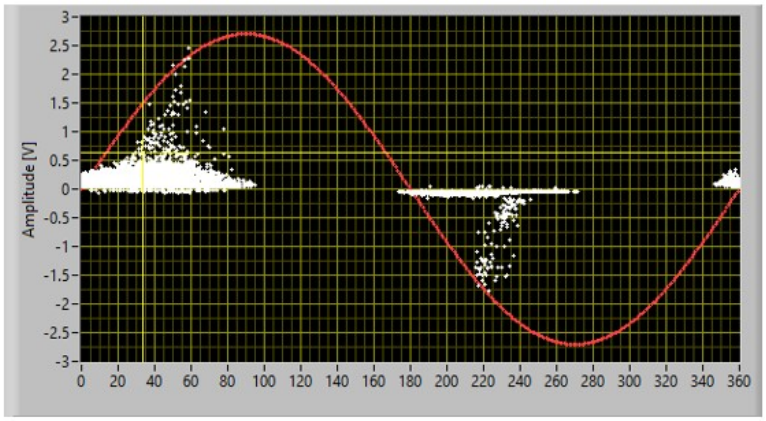

(a)

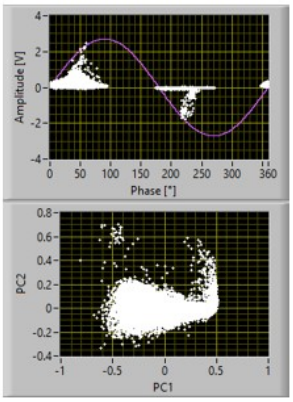

(b)

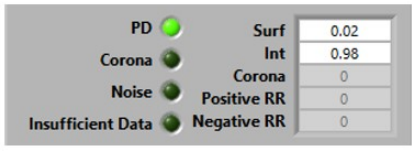

(c)

Figure 4.14: (a) Kapton NCR Phase-resolved PD (PRPD) pattern (b) separation (PCA) map (c) Identification in the end of aging (t=4.5) for 2kV

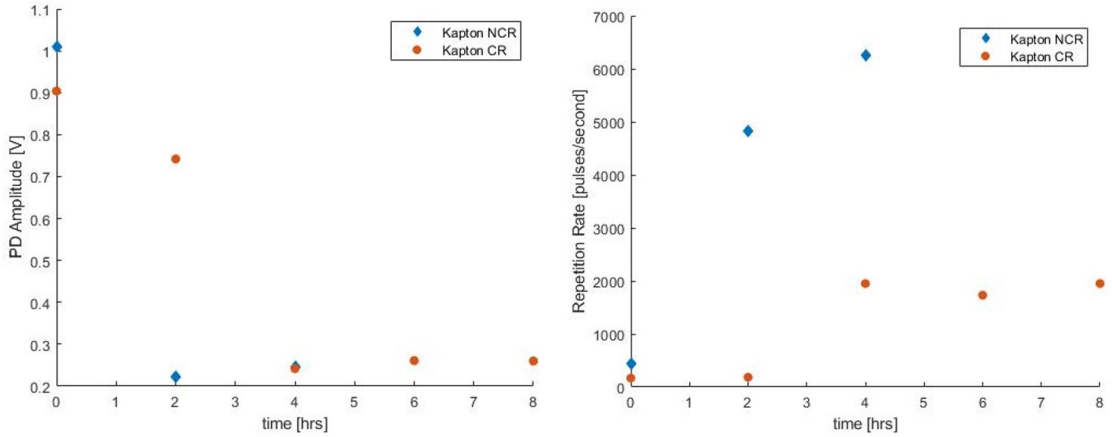

(a) (b)

Figure 4.15: Partial Discharge 95% Confidence Partial Discharge amplitude (a) and partial discharge repetition rate (b) for Kapton CR and NCR at 2kV

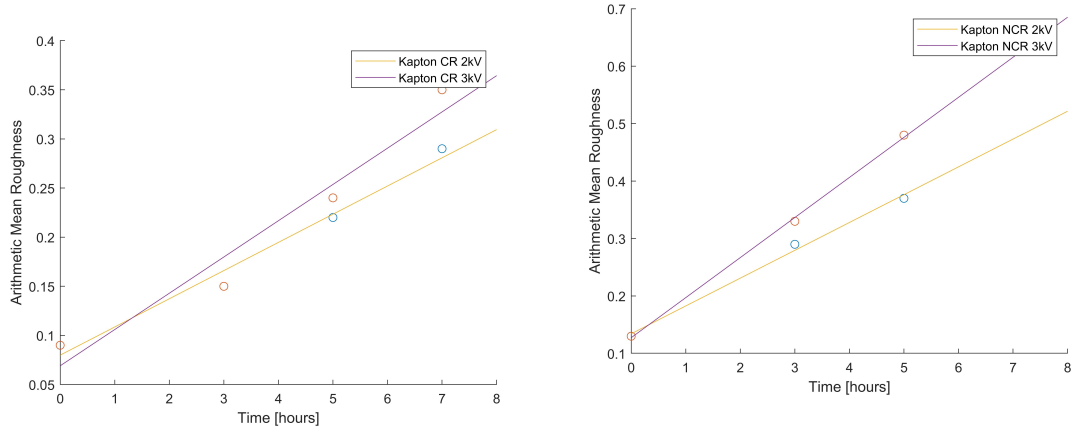

(a) (b)

Figure 4.16: Surface Roughness for Kapton CR (a) and Kapton NCR (b) at 2kV

4.3.3 Visual Inspection

The last form of erosion test analysis of the erosion tests were from visual inspection using a microscope with 720x and 2040x magnification. Figures 4.17, 4.18, and 4.19 show the impact of erosion for Kapton NCR. Pitting is significant even after 2.5 hours, and is significantly larger at 5 hours with failure occurring shortly after. Figures 4.20, 4.21, 4.22, and 4.23 show the images of Kapton CR. The result of the erosion is first seen as a bi-product on the surface of the sample with some pitting (but much less than Kapton NCR at any time). The observed degradation of Kapton CR matches with the previous results and is quite small.

In summary, these tests provide an effective method for rapid material characterization which can provide valuable insight into material performance. While Kapton NCR has a 10% larger breakdown strength its ability to endure partial discharge is significantly lower when compared to corona resistant Kapton.

4.4 Dynamic Health Index

The results of the surface erosion can be applied to produce a metric for condition based monitoring. Results of measured partial discharge patterns and associated metrics can be organized into a dynamic health index which can be used to asses the condition of insulation systems. In general a health index converts any observed aging observation to a metric which provides the relative health (in percent) of the asset. A dynamic health index is based on the same principle with the additional requirement of online measurements.A Dynamic Health Index (DHI) can be used for any class of aging phenomena (partial discharge, thermal degradation, or mechanical). [26]

As a general approach to DHI, a class, j (e.g. partial discharge, thermography, watertreeing, etc.), for an insulation sub-system, i (e.g. bushing, transformer winding, auxiliary solid insulation, etc.), can be structured with k diagnostic markers (e.g. partial discharge amplitude, repetition rate, identification, etc.), each associated to a score $S_{(i,j,k)}$. As an example, $S_{(i,j,k)}$ = 1-5, from best to worst conditions. Furthermore, a weight, $W_{(i,j,k)}$. A, could be attributed to each diagnostic marker, depending on its harmfulness in terms of aging rate and breakdown processes. The more the specific diagnostic marker is associated with an aging mechanism which has a fast degradation rate, the larger will be its weight.
A dynamic health index has been defined by Montanari et al in [26]

$$DHI(t) = \prod_i \left(1 - \frac{W_{avg,i,j} SC_{min,j}}{SC_{max,j} - SC_{min,j}}\right) \tag{4.4}$$

Where where $SC_{max,j}$ and $SC_{min,j}$ are the maximum and minimum scores for the observed diagnostic

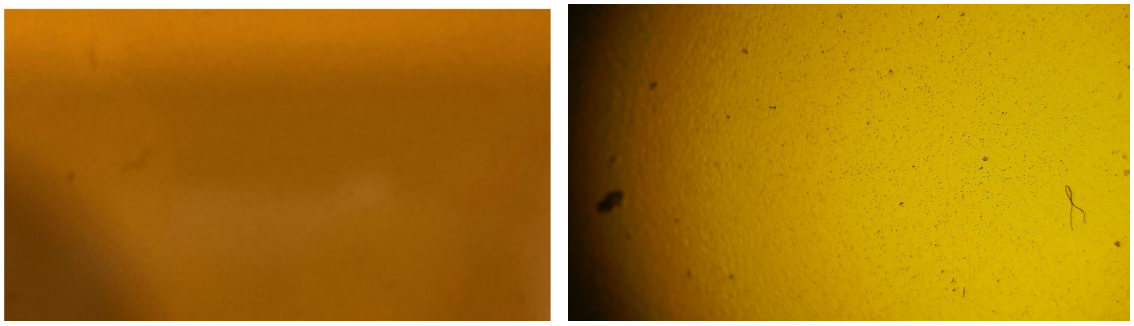

(a) (b)

Figure 4.17: Kapton NCR after 0hrs of Aging with (a) 600x Magnification (b) and 2040x Magnification

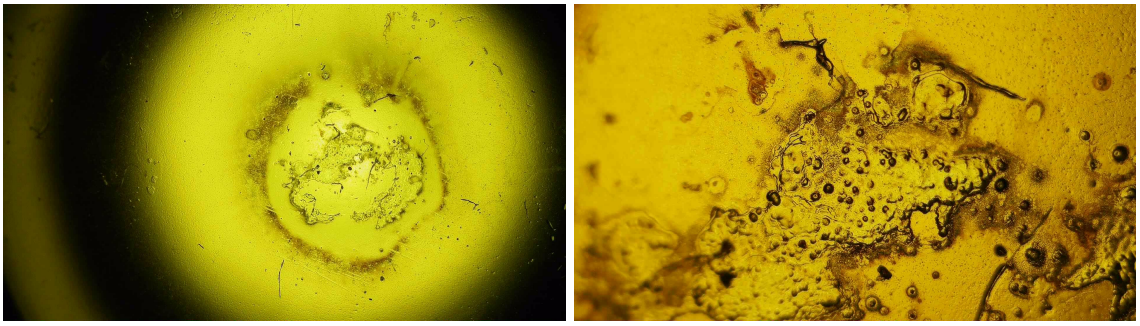

(a) (b)

Figure 4.18: Kapton NCR after 3hrs of Aging with (a) 600x Magnification (b) and 2040x Magnification

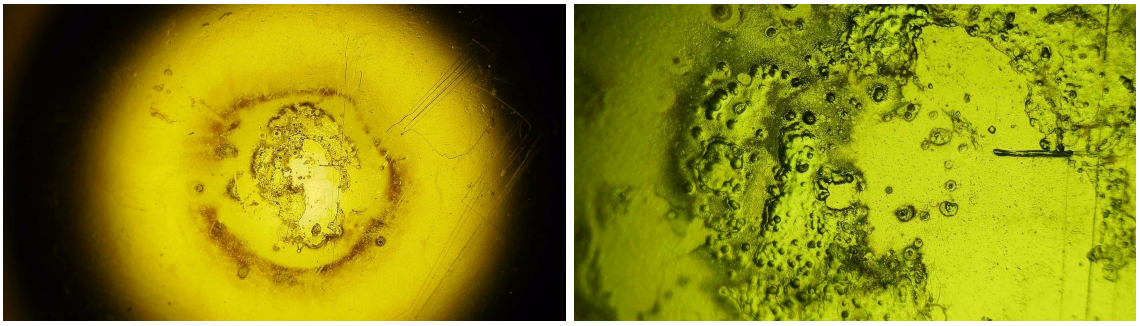

(a) (b)

Figure 4.19: Kapton NCR after 5hrs of Aging with (a) 600x Magnification (b) and 2040x Magnification

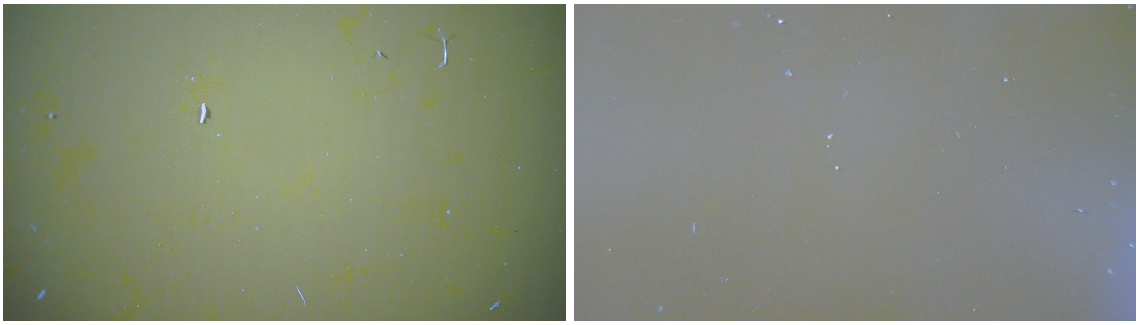

(a) (b)

Figure 4.20: Kapton CR after 0hrs of Aging with (a) 600x Magnification (b) and 2040x Magnification

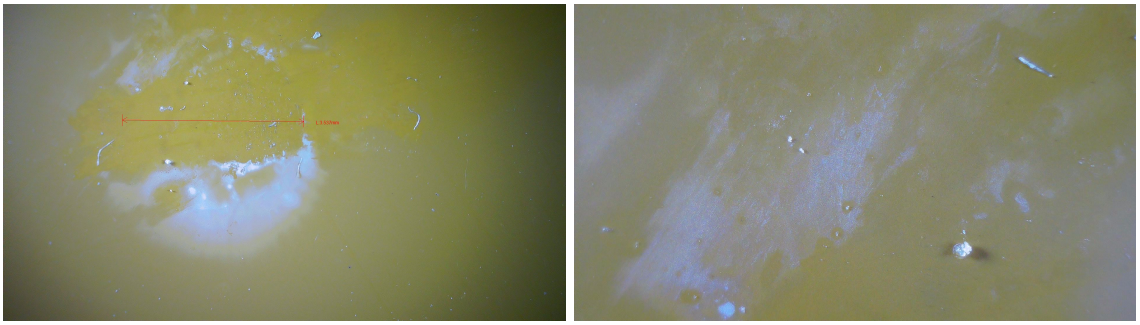

(a) (b)

Figure 4.21: Kapton CR after 3hrs of Aging with (a) 600x Magnification (b) and 2040x Magnification

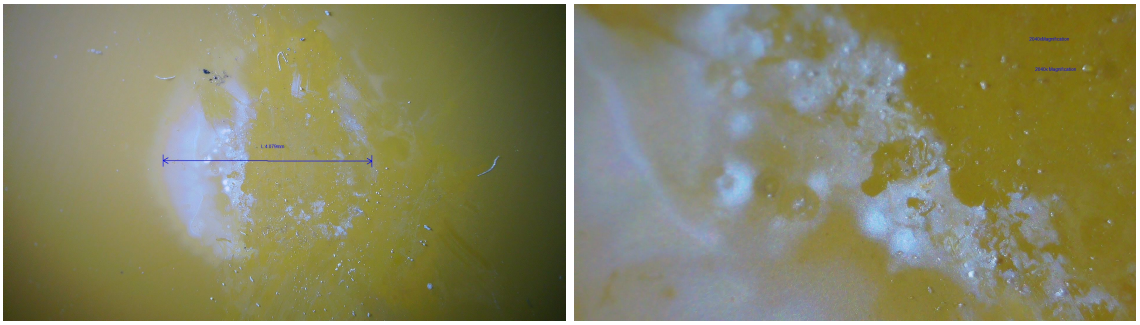

(a) (b)

Figure 4.22: Kapton CR after 5hrs of Aging with (a) 600x Magnification (b) and 2040x Magnification

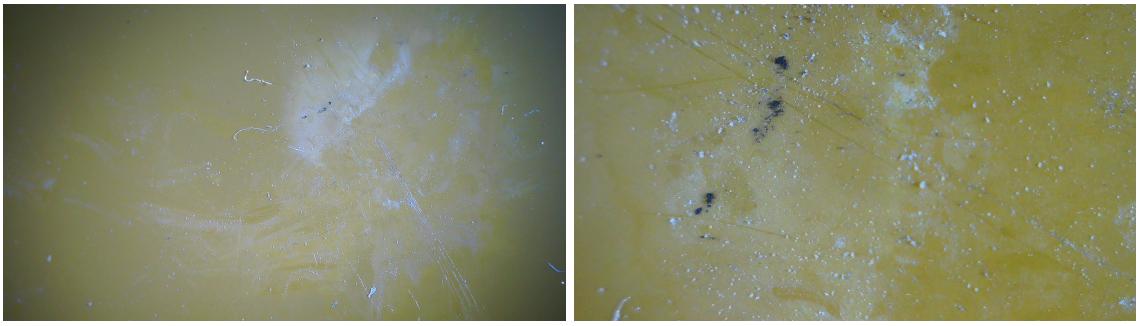

(a) (b)

Figure 4.23: Kapton CR after 7hrs of Aging with (a) 600x Magnification (a) and 2040x Magnification

marker, $W_{avg,i,j}$ is the weighted average defined as:

$$W_{avg}(t) = \frac{\sum_{k=1}^{2} S_k W_k}{\sum_{k=1}^{2} W_k} \tag{4.5}$$

And the diagnostic marker defined for partial discharge as:

$$S_k(t) = P_k(t) \frac{A(t) RR(t)}{A_0 RR_0} \tag{4.6}$$

Where k is equal to 2, (1 = surface discharge and 2 = internal discharge) then P_k then becomes the percent identified as the respective source of partial discharge. A is 95% confidence internal for the partial discharge amplitude, and A_0 is a reference amplitude. RR is the repetition rate of the partial discharge and RR_0 is a reference repetition rate. In this analysis only partial discharge is analyzed as a diagnostic marker and only one sub component which results in the definition of the dynamic health index as:

$$DHI(t) = 1 - \frac{W_{avg}(t)}{SC_{max} - 1} \tag{4.7}$$

This dynamic health index can also be mapped directly to a life estimate:

$$L_R = \left(1 - \frac{t_i}{L_D}\right) L_D = DHI \cdot L_D \tag{4.8}$$

Where L_R is the residual life of the asset under analysis, L_D is the design life at the commissioning of the asset and t_i is the time aging has been experienced. Of note regarding the surface erosion testing is the identification transition from mostly surface discharge to mostly internal which in terms of the dynamic health index is a transition from a lower weighted phenomena to a higher weighted phenomena marking the larger impact on aging. The surface erosion testing is shown in Figure 4.24 which shows that based purely on

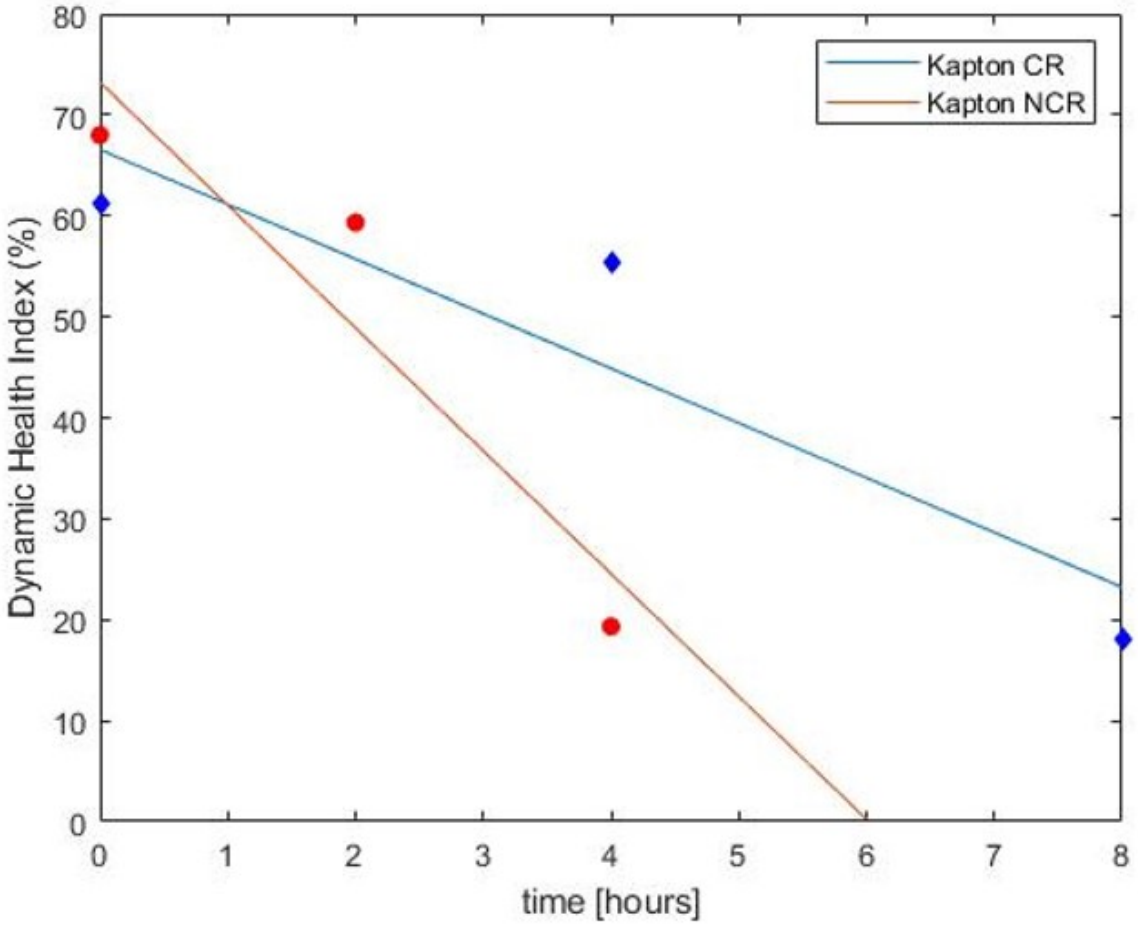

Figure 4.24: Dynamic Health index for Kapton CR and Kapton NCR

the observed partial discharge pattern in combination with the dynamic health index algorithm an effective estimate of life can be implemented. Early on while partial discharge is present the level of erosion and impact on the insulation system is small and a maintenance action may not be needed.

Chapter 5

Conclusion

In summary, this thesis provides the characterization of a laminated bus bar. With the analytical basis of a recently proposed model for surface discharge. The results of this analysis show that the traditional concept of creepage is not equivalent with ensuring a surface discharge free design. Under AC conditions the experiential results prove that PD will occur at voltages below the nominal operating voltage for the given creepage distance. Even if the creepage and clearance requirements are met, insulation degradation can still occur. In the case of the laminated bus bar due to the terminal designs and the triple point geometry a significant, non-uniform electric field is present. Instead of relying on general rules to minimize the electric field, employing the surface discharge model can allow for more precise calculation and evaluation respecting partial discharge inception voltage. Note this approach is not a reason to replace the standards, surface discharge theory and simulations can be employed as an additional way to ensure a partial discharge free design.

During the design process choices must be made for the insulation selected, the selection is often based on a materials relative permittivity, dielectric strength, and thermal conductivity to name a few. As a result of recent developments nanomaterials which can endure partial discharge are now a design option. This work explores an alternative method for rapid material characterization on commercial Kapton NCR and Kapton CRC. It is always important to design an insulation system such that no partial discharge is present during nominal operation. However, in many cases partial discharge could be incepted as a result of environmental factors. This factor motivates the use of materials which can endure partial discharge during these conditions, and thus a method which can rapidly compare materials in this regard.

Additional results from conducting surface erosion testing provide the foundation for a health index which can be employed in conjunction with online monitoring. The purpose of the health index is to convert

measured quantities into a simple metric for life estimation. This conversion was allowed as a result of the changes in the phase resolved partial discharge pattern vs sample aging.

5.1 Future Work

The primary basis for future work is incorporation of the surface discharge model into a virtual prototyping process. Previous work has incorporated standards-based insulation coordination into the process. [10] It is the next step to add physics based rules for insulation coordination, especially in a framework for multi objective optimization. To achieving this goal will require employing computationally efficient methods for electric field simulation. This work has laid the foundation of physics based modeling applied to a laminated bus bar, this same modeling approach can be applied generally to insulation designs.

Bibliography

[1] en. In: *IEC 61800-5-1*. UK: British Standards, 2007.

[2] J.M. Allocco. "Laminated bus bars for power system interconnects". In: *IEE Colloquium on Passive Components for Power Electronic Systems (Digest No. 1998/261)*. 1998, pp. 5/1–5/7. DOI: 10.1049/ic:19980352.

[3] Küchler Andreas. *High Voltage Engineering Fundamentals - technology - applications*. de. Berlin: Springer Vieweg, 2018.

[4] S. Boggs. "Very high field phenomena in Dielectrics". en. In: *IEEE Transactions on Dielectrics and Electrical Insulation* 12.5 (2005), pp. 929–938.

[5] S.A. Boggs. "Partial discharge: Overview and signal generation". en. In: *IEEE Electrical Insulation Magazine* 6.4 (1990), pp. 33–39.

[6] A. Cavallini, D. Fabiani, and G.C. Montanari. "Time-evolution of nanostructured epoxy resin degradation due to surface partial discharge activities". en. In: *2007 Annual Report - Conference on Electrical Insulation and Dielectric Phenomena*. 2007.

[7] J.-S. Chang, P.A. Lawless, and T. Yamamoto. "Corona Discharge Processes". fr. In: *IEEE Transactions on Plasma Science* 19.6 (1991), pp. 1152–1166.

[8] F.-C. Chiu. "A review on conduction mechanisms in dielectric films". en. In: *Advances in Materials Science and Engineering* 2014 (2014), pp. 1–18.

[9] G.C. Crichton, P.W. Karlsson, and A. Pedersen. "Partial discharges in ellipsoidal and spheroidal voids". In: *IEEE Transactions on Electrical Insulation* 24.2 (1989), pp. 335–342. DOI: 10.1109/14.90292.

[10] R.M. Cuzner and W.J. Koebel. "Application of IEC-61800-5 insulation coordination to shipboard equipment scaling studies". en. In: *2021 IEEE Electric Ship Technologies Symposium (ESTS*. 2021.

[11] Robert Cuzner, Mark Vygoder, and Rounak Siddaiah. "Power Conversion and Distribution Equipment Metamodels for Dependable Design of Shipboard Integrated Power and Energy Systems". In: *2018 IEEE International Conference on Electrical Systems for Aircraft, Railway, Ship Propulsion and Road Vehicles & International Transportation Electrification Conference (ESARS-ITEC)*. 2018, pp. 1–8. DOI: 10.1109/ESARS-ITEC.2018.8607676.

[12] L.A. Dissado, G. Mazzanti, and G.C. Montanari. "The role of trapped space charges in the electrical aging of insulating materials". en. In: *IEEE Transactions on Dielectrics and Electrical Insulation* 4.5 (1997), pp. 496–506.

[13] R. Ghosh, G.C. Montanari, and P. Seri. "Increasing grid and asset resilience: An Automatic and unsupervised approach to partial discharge monitoring in Cables". en. In: *2021 IEEE Power & Energy Society General Meeting (PESGM*. 2021.

[14] R. Ghosh, P. Seri, and G.C. Montanari. "Measuring PD under fast slew rate, high voltage and high frequency repetitive voltage impulses". en. In: *2020 IEEE 15th International Conference on Industrial and Information Systems (ICIIS*. 2020.

[15] R. Ghosh et al. "Noise rejection and detection of partial discharges under Repetitive Impulse Supply Voltage". en. In: *IEEE Transactions on Industrial Electronics* 67.5 (2020), pp. 4144–4151.

[16] C. Heitz. "A general stochastic approach to partial discharge processes". en. In: *ICSD'98. Proceedings of the 1998 IEEE 6th International Conference on Conduction and Breakdown in Solid Dielectrics (Cat.* No.98CH36132.

[17] G. Hoogenraad, P.H.F. Morshuis, and C. Petrarca. "Classification of partial discharges for DC Equipment". en. In: *Proceedings of Conference on Electrical Insulation and Dielectric Phenomena - CEIDP '96.*

[18] C. Hudon et al. "Using integrated generator diagnosis to perform condition based maintenance". en. In: *2015 IEEE Electrical Insulation Conference (EIC.* 2015.

[19] "IEEE Standard for Insulation Coordination–Definitions, Principles, and Rules". In: *IEEE Std C62.82.1-2010 (Revision of IEEE Std 1313.1-1996)* (2011), pp. 1–22. DOI: 10.1109/IEEESTD.2011.5754137.

[20] G. Jiang, J. Kuang, and S. Boggs. "Critical parameters for electrical tree formation in XLPE". en. In: *IEEE Transactions on Power Delivery* 13.2 (1998), pp. 292–296.

[21] C. Laurent et al. "Charge Dynamics and its energetic features in polymeric materials". en. In: *IEEE Transactions on Dielectrics and Electrical Insulation* 20.2 (2013), pp. 357–381.

[22] G. Mazzanti, G.C. Montanari, and L.A. Dissado. "Electrical aging and life models: The role of space charge". en. In: *IEEE Transactions on Dielectrics and Electrical Insulation* 12.5 (2005), pp. 876–890.

[23] H.C. Miller. "Surface flashover of insulators". en. In: *IEEE Transactions on Electrical Insulation* 24.5 (1989), pp. 765–786.

[24] G.C. Montanari, R. Ghosh, and P. Seri. "HV and MV DC insulation system: Unexpected aging mechanisms and metrics for life prediction". en. In: *2020 IEEE 15th International Conference on Industrial and Information Systems (ICIIS.* 2020.

[25] G.C. Montanari, Skyler Schwartz, and Pasquale Cambareri. "Partial Discharge Free Design of Electrical Insulation Systems: an Application to Laminated Busbars for Ship Assets". In: 2023.

[26] G.C. Montanari, Skyler Schwartz, and Robert Cuzner. "A Dynamic Health Index approach for aviation electrical assets based on the detection of partial discharges and their harmfulness". In: 2023.

[27] G.C. Montanari, Skyler Schwartz, and Robert Cuzner. "On the Characterization of Partial-Discharge Endurance of Dielectric Materials for Aerospace Applications". In: 2023.

[28] G.C. Montanari and L. Simoni. "Aging phenomenology and modeling". en. In: *IEEE Transactions on Electrical Insulation* 28.5 (1993), pp. 755–776.

[29] G.C. Montanari et al. "An Accelerated Testing Procedure to Evaluate and Compare the Resistance to Partial Discharges of Insulating Materials for Electrified Transportation Assets". In: 2023.

[30] G.C. Montanari et al. "An approach to insulation condition monitoring and life assessment in Emerging Electrical Environments". en. In: *IEEE Transactions on Power Delivery* 34.4 (2019), pp. 1357–1364.

[31] G.C. Montanari et al. "Innovative Design of Laminated Bus Bars for Electrical Ships: Three-Leg Approach". In: 2023.

[32] G.C. Montanari et al. "Noise rejection and partial discharge source identification in insulation system under DC voltage supply". en. In: *IEEE Transactions on Dielectrics and Electrical Insulation* 26.6 (2019), pp. 1894–1902.

[33] G.C. Montanari et al. "On the likelihood of partial discharge inception in laminated busbars from electrified ships". en. In: *2021 IEEE Electric Ship Technologies Symposium (ESTS).* 2021.

[34] G.C. Montanari et al. "The dimensional approach in the design and qualification tests of AC and DC HV Cables: The OCCHINI approach revisited". en. In: *IEEE Transactions on Power Delivery* 35.5 (2020), pp. 2119–2126.

[35] H. Naderiallaf, P. Seri, and G.C. Montanari. "Effect of voltage slew rate on partial discharge phenomenology during voltage transient in HVDC insulation: The case of polymeric cables". en. In: *IEEE Transactions on Dielectrics and Electrical Insulation* 29.1 (2022), pp. 215–222.

[36] D. Nath et al. "Modeling and characterization of surface discharges in insulating material for spacers: Electrode Shape, discharge mode, and revision of the creepage concept". en. In: *Materials* 16.3 (2023), p. 989.

[37] L. Niemeyer. "A generalized approach to partial discharge modeling". en. In: *IEEE Transactions on Dielectrics and Electrical Insulation* 2.4 (1995), pp. 510–528.

[38] H. Niu et al. "Noise rejection strategy and experimental research on partial discharge at DC Voltage". en. In: *2009 IEEE 9th International Conference on the Properties and Applications of Dielectric Materials*. 2009.

[39] J.J. O'Dwyer. "The role of space charge in the theory of solid-dielectric breakdown". en. In: *Conference on Electrical Insulation & Dielectric Phenomena — Annual Report 1983*. 1983.

[40] C. Park. "Electret: An entirely new approach of solving partial discharge caused by triple points, sharp edges, bubbles, and airgaps". en. In: *IEEE Access* 8 (2020), pp. 78354–78366.

[41] C. Park. "Electrets: A remedy for partial discharge caused by Power Electronics switching". en. In: *IEEE Transactions on Industrial Electronics* 68.12 (2021), pp. 12947–12952.

[42] P. Seri, R. Ghosh, and G.C. Montanari. "An unsupervised approach to partial discharge monitoring in rotating machines: Detection to diagnosis with reduced need of expert support". en. In: *IEEE Transactions on Energy Conversion* 36.3 (2021), pp. 2485–2492.

[43] P. Seri, H. Naderiallaf, and G.C. Montanari. "Modelling of supply voltage frequency effect on partial discharge repetition rate and charge amplitude from AC to DC at room temperature". en. In: *IEEE Transactions on Dielectrics and Electrical Insulation* 27.3 (2020), pp. 764–772.

[44] P. Seri et al. "An approach to noise rejection and partial discharge separation in DC cable testing, during steady state and voltage polarity inversion transients". en. In: *2020 8th International Conference on Condition Monitoring and Diagnosis (CMD*. 2020.

[45] T. Tanaka et al. "Proposal of a multi-core model for polymer nanocomposite dielectrics". In: *IEEE Transactions on Dielectrics and Electrical Insulation* 12.4 (2005), pp. 669–681. DOI: 10.1109/TDEI.2005.1511092.

[46] G. Teyssedre and C. Laurent. "Charge transport modeling in insulating polymers: From molecular to macroscopic scale". en. In: *IEEE Transactions on Dielectrics and Electrical Insulation* 12.5 (2005), pp. 857–875.

[47] "UL Standard for Safety Systems of Insulating Materials – General". In: *UL1446* (2019), pp. 1–51.